

## DNS-based predictive control of turbulence: an optimal benchmark for feedback algorithms

By THOMAS R. BEWLEY<sup>1,2</sup>,  
PARVIZ MOIN<sup>2</sup> AND ROGER TEMAM<sup>3</sup>

<sup>1</sup>Department of Mechanical and Aerospace Engineering, University of California San Diego,  
La Jolla, CA 92093, USA

<sup>2</sup>Center for Turbulence Research, Stanford University, Stanford, CA 94305, USA

<sup>3</sup>Laboratoire d'Analyse Numérique, Université de Paris-Sud, 91405 Orsay, France  
and The Institute for Scientific Computing and Applied Mathematics, Indiana University,  
Bloomington, IN 47405, USA

(Received 13 August 1999 and in revised form 30 May 2001)

Direct numerical simulations (DNS) and optimal control theory are used in a predictive control setting to determine controls that effectively reduce the turbulent kinetic energy and drag of a turbulent flow in a plane channel at  $Re_\tau = 100$  and  $Re_\tau = 180$ . Wall transpiration (unsteady blowing/suction) with zero net mass flux is used as the control. The algorithm used for the control optimization is based solely on the control objective and the nonlinear partial differential equation governing the flow, with no *ad hoc* assumptions other than the finite prediction horizon,  $T$ , over which the control is optimized.

Flow relaminarization, accompanied by a drag reduction of over 50%, is obtained in some of the control cases with the predictive control approach in direct numerical simulations of subcritical turbulent channel flows. Such performance far exceeds what has been obtained to date in similar flows (using this type of actuation) via adaptive strategies such as neural networks, intuition-based strategies such as opposition control, and the so-called ‘suboptimal’ strategies, which involve optimizations over a vanishingly small prediction horizon  $T^+ \rightarrow 0$ . To achieve flow relaminarization in the predictive control approach, it is shown that it is necessary to optimize the controls over a sufficiently long prediction horizon  $T^+ \gtrsim 25$ . Implications of this result are discussed.

The predictive control algorithm requires full flow field information and is computationally expensive, involving iterative direct numerical simulations. It is, therefore, impossible to implement this algorithm directly in a practical setting. However, these calculations allow us to quantify the best possible system performance given a certain class of flow actuation and to qualify how optimized controls correlate with the near-wall coherent structures believed to dominate the process of turbulence production in wall-bounded flows. Further, various approaches have been proposed to distil practical feedback schemes from the predictive control approach without the suboptimal approximation, which is shown in the present work to restrict severely the effectiveness of the resulting control algorithm. The present work thus represents a further step towards the determination of optimally effective yet implementable control strategies for the mitigation or enhancement of the consequential effects of turbulence.

---

## 1. Background

The recent development of the technology necessary to produce micro-scale mechanical devices, commonly referred to as micro-electro-mechanical systems (MEMS), has prompted researchers to investigate the possibility of using micro-scale actuation for the control of unstable flow phenomena in order to achieve macro-scale effects. Such leveraging of control effort is possible in chaotic systems (such as turbulence) due to the extreme sensitivity of such systems to small levels of control forcing. Of primary interest in such problems, of course, is the determination of when and where control should be applied to maximize the desired effect.

The original vision for the emergence of MEMS was given by Richard Feynman (1959), in his classic lecture at the American Physical Society entitled ‘There’s Plenty of Room at the Bottom’, in which Feynman foresaw many of the techniques and challenges encountered by the MEMS community today. Building on the technology developed for the fabrication of silicon chips, there has been a flurry of activity in MEMS for the last decade. For reviews of recent developments of MEMS technology which relate to micro-scale measurement and control in fluid mechanics, the reader is referred to Ho & Tai (1996, 1998), McMichael (1996), Gad el Hak (1996), and Moin & Bewley (1994). In these reviews, the reader will find a variety of sensors and actuators currently under development which are suitable for application in feedback control of turbulence. The primary questions in MEMS development today are how to design such devices to be durable in hostile environments and how to produce such devices at high yield and low cost.

Suffice it to say here that, in the near future, it might be possible to use MEMS technology to measure small-scale turbulent fluctuations of a flow and, subsequently, to apply coordinated small-scale forcing to the flow in order to achieve a desired large-scale effect. Examples of problems of particular interest include reducing drag, reducing heat transfer, delaying transition, delaying separation, increasing mixing, and reducing levels of wall-pressure fluctuations and/or radiated sound. For each of these problems, important questions arise:

1. How much do practical engineering designs stand to benefit if durable MEMS sensors and actuators can indeed be built in large arrays?
2. How and where should the control be applied?
3. Is feedback necessary? If so, what attainable flow field measurements provide the most useful information? What feedback algorithms are most effective? Specifically,
  - (i) Are simple output feedback rules sufficient, or is low-order state estimation required?
  - (ii) Is linear feedback effective for the control and estimation problems, or is a gain scheduling approach and/or some form of nonlinear feedback preferable?

Answers to most of these questions are not yet known. The present work implements a sensitivity analysis of the Navier–Stokes equation through the definition of an *adjoint field*. From this type of analysis, answers to some of these questions may begin to be sought. As discussed in Bewley (2001) and Bewley *et al.* (2000), the approach used in the present paper may be extended readily to a variety of problems in fluid mechanics, including the optimization of open-loop time-periodic forcing profiles for turbulent jets and the forecasting of chaotic fluid systems based on limited noisy flowfield measurements. Thus, the approach being developed is of interest even if vast arrays of durable MEMS devices are never realized for commercial use.

We now summarize a few of the recent approaches used to determine implementable feedback control algorithms for turbulent flows, categorizing these approaches to

the feedback control problem by examining their mathematical dependence on the equation governing the system. This brief survey of this active field of research puts the present approach in context with a sampling of the other techniques currently under investigation. For a more thorough discussion along this line, see Moin & Bewley (1994).

### 1.1. Adaptive networks

The first class of schemes which may be proposed to achieve small-scale flow control actually makes no explicit reference to the dynamics known to take place in the flow or the Navier–Stokes equation which governs these dynamics. Instead, a ‘reasonable’ network is fashioned which takes as input those measurable flow quantities assumed to be most relevant to the control problem and produces as output the requisite control velocity. The coefficients of this network are then ‘trained’ by applying the control network to the flow and gradually adjusting the coefficients in a heuristic manner based on the resulting evolution of the flow. (Note that there are many different approaches to adaptive control. Hertz, Krogh & Palmer 1991 and Ioannou & Sun 1996 discuss several possible techniques.) The main advantage of the adaptive approach is that the feedback coefficients can adjust to compensate for changing characteristics of the system being controlled, such as modification of the mean flow speed and direction, the sensitivity of the sensors, and the responsiveness of the actuators.

As an example of one adaptive approach, an adaptive inverse technique has been applied by Lee *et al.* (1997) to a turbulent channel flow at  $Re_\tau = 100$ , providing approximately 20% drag reduction. This approach first develops an approximate ‘inverse model’ between measurable flow quantities (as input) and the control forcing (as output) with an adaptive technique. This is done by forcing the system with small, ‘sufficiently rich’ control signals which ‘push’ the system in a variety of different directions while monitoring the responses of the measurements. From these data, a network is constructed which attempts to reproduce (model) the control used based on the measurements taken. (In an inherently nonlinear system such as turbulence, this is a challenging proposition, as any simple linear expression of this relationship would probably be highly non-stationary as the arrangement of the coherent structures near the wall evolves in time.) Each iteration of the adaptation for this inverse model consists of three steps: (1) computing the error of the model output with respect to the desired model output (the actual control forcing used), (2) determining the influence of the various weights in the model on this error, then (3) updating all the weights in the model a small amount in a manner that reduces the error. When applied to the nonlinear adaptive networks commonly used for this purpose, known as ‘neural networks’, this is referred to as ‘back-propagation’ of the error. Once (if) the approximate inverse model between the flow measurements and the control converges for the open-loop system, the inverse model is used to determine a control which will drive the flow measurements towards some desired state. This control is then applied to the flow, and the inverse model is further trained to adapt it to the (now modified) characteristics of the closed-loop system. In the case of Lee *et al.* (1997), the desired state was chosen to be a state with reduced fluctuations of the spanwise wall shear. Several other strategies may be considered and lead to schemes of varying degrees of effectiveness.

### 1.2. Schemes based on understanding of dominant physics

In situations in which the dominant physics is well understood, judgment can guide an engineer to design effective control schemes. Success is limited, however, by the

engineer's understanding of the physical processes involved; in the case of turbulence, our understanding is still limited despite several decades of intense research.

As an example, an opposition strategy was used by Choi, Moin & Kim (1994) to reduce the drag in a turbulent channel flow at  $Re_\tau = 100$  by mitigating the effect of the near-wall vortices. By opposing near-wall vertical motions of the fluid with an equal and opposite control velocity at the wall, the motion of high-momentum fluid towards the wall by the sweep events is abated, and the drag may be reduced by up to 25%.

In follow-on computations and flow visualizations by Hammond, Bewley & Moin (1998) at  $Re_\tau = 180$ , it was shown why this opposition strategy is effective only when the distance  $y$  between the detection plane and the wall is sufficiently small ( $y^+ = 15$  works best). When the detection plane is too far from the wall, high-speed fluid may be drawn in *on a skewed path* from a sweep event into the near-wall region and down towards the wall beneath a nearby ejection event, where the opposition scheme applies suction. For  $y^+ > 15$ , this mechanism of instability of the closed-loop system is possible, and the turbulence levels and mean drag of the flow are significantly increased. For  $y^+ \lesssim 15$ , the detection plane is too close to the wall for this mechanism of instability to be effective (as viscosity limits the cross-flow convection possible immediately adjacent to the wall), and the turbulence levels and mean drag are reduced.

Another promising intuition-based concept was proposed by Koumoutsakos (1997), in which the turbulence control problem is considered in terms of the minimization of the so-called 'vorticity flux' (i.e. the wall-normal component of the vorticity gradient tensor) at the wall. The control algorithms considered in this framework may be constrained at the outset to depend on wall information only. The simulations of Koumoutsakos (1999) of a turbulent channel flow at  $Re_\tau = 180$  indicate the formation of sustained spanwise-coherent fluid 'rollers' near the wall with wall-normal blowing/suction via a control strategy targeting reduced gradients of vorticity near the wall. Drag reductions of 40% are reported. A related strategy has been proposed by Keefe (1997) in which the wall-normal gradients of wall-normal vorticity are reduced via the selective actuation of an array of small rotatable disks flush-mounted on the surface rather than a distribution of blowing/suction. Such a configuration might be more straightforward to implement in hardware than blowing/suction. Related channel-flow simulations, in which body forcing confined to the  $x_2^+ < 6$  region was used instead of boundary forcing, have resulted in drag reductions of up to 35% (Keefe 1995).

### 1.3. Extrapolation of linear control theory

The application of linear control theory to the linearized Navier–Stokes equation in a channel is straightforward: see, e.g. Joshi, Speyer & Kim (1997) for the application of classical control theory and Bewley & Liu (1998) for the application of modern control theory. There are a few critical issues concerning the development of practically implementable algorithms which are still being addressed, but these do not appear to be insurmountable.

One of the most important such issues is that the weights in the linear feedback controller must have compact support in physical space (even if it is designed in Fourier space) in order for the controller to be implementable (Bamieh 1997). It is important to note that many linear controllers designed in Fourier space do not satisfy this property. In flows which are not spatially periodic (as is the case with all real channel flows), an incorrect assumption of spatial periodicity in the

application of a non-compact controller would result in a Gibbs phenomenon which would probably render the controller ineffective even if all other assumptions in the controller design were met in the experiment. On the other hand, a physical-space controller with compact spatial support is not affected by Gibbs phenomenon and therefore generalizes to a variety of periodic and non-periodic flows with similar near-wall dynamics.

Another important issue yet to be completely resolved is the most appropriate method for linear model reduction. Cortelezzi *et al.* (1999) addresses this topic and obtains a linear model reduction by truncating those linear eigenmodes with low observability or controllability from a model of a two-dimensional unsteady channel flow. (Surprisingly, Cortelezzi *et al.* 1999 reports a drag reduction to 50% below the laminar level by application of a zero-net-mass-flux linear controller.) In the highly non-orthogonal (i.e. nearly defective) systems often encountered in three-dimensional flows, model reduction schemes that take into account the transfer function of interest, such as the  $p, q$  Markov covariance equivalent realization (Villemagne & Skelton 1988) or optimal Hankel norm approximation (Zhou, Doyle & Glover 1996), are well suited, and should be studied in future work.

Even with such questions remaining open, researchers are beginning to consider the extrapolation of the linear control feedback determined by linear control theory directly to the fully nonlinear problem of a turbulent flow. The first reason to try such an approach is simply because we can: due to the ease of determining and implementing linear control feedback, we should attempt to exploit everything we can from our ability to compute linear controls.

There is at least some justification in the fluids literature for such an approach. Though the significance of this result has been debated, Farrell & Ioannou (1993) have clearly shown that the linearized Navier–Stokes equation in a plane channel flow, when excited with the appropriate stochastic forcing, exhibits behaviour which is reminiscent of the streamwise vortices and streamwise streaks characteristic of turbulent flows, though perhaps at a length scale which must be tuned by observation of the full nonlinear system. Whatever information the linearized equation actually contains about the real mechanisms for formation of streamwise vortices and streamwise streaks, the linear controllers should be able to exploit.

There is also some justification in the mathematical literature for such an approach. Interestingly, Barbu & Sritharan (1998) proved mathematically that solutions of the linear robust control problem for Navier–Stokes systems, such as those determined by Bewley & Liu (1998) for small perturbations to a laminar channel flow, are  $\gamma$ -suboptimal for the full (nonlinear) Navier–Stokes equation for finite (albeit sufficiently small) flow perturbations. However, important possible pitfalls of applying linear control feedback to stabilize *large* flow perturbations, such as those on a chaotic attractor (where the effects of the nonlinear terms are essential for describing the system behaviour), are illustrated for a simple model problem by Bewley (1999). It is shown in this reference that such an approach can lead to closed-loop systems which can either converge to the wrong state or even blow up unless the appropriate nonlinear switches are introduced.

#### 1.4. *A need for reduced-order nonlinear models*

When considering the control of the multi-scale phenomenon of turbulence, it is clear that an accurate reduced-order nonlinear model (as an alternative to direct numerical simulation) would simplify the control problem greatly. At the very least, an efficient reduced-order *representation* of the near-wall turbulent state is probably necessary

if we are ever to attempt to implement an estimator-based control algorithm, as discussed in §2.4, even if the dynamics of such a reduced-order model does not follow closely the dynamics of the full Navier–Stokes system without substantial measurement feedback. Such reduced-order models for turbulent flows have been sought for years, though the suitability of current approaches for providing such models for a *controlled* turbulent flow (for which the dynamics is substantially altered from that of the uncontrolled turbulent flow) is still an open question.

In the framework of a reduced-order model, the movement of the near-wall longitudinal vortices when observed in a cross-flow plane is interpreted as the orbiting of a low-dimensional state. The complete passage of a coherent structure through the cross-flow plane of interest leads to a rapid jump in this state to a different state, representing a modified distribution of near-wall longitudinal vortices. Such a rapid jump between critical points (sometimes referred to in the fluids literature as a so-called ‘turbulent burst’), followed by a quiescent period in which the flow pattern remains largely unchanged, is referred to in the dynamical systems literature as a heteroclinic cycle. With a good reduced-order model, one might hope to characterize the quiescent period, as the longitudinal legs of the near-wall coherent structures convect through a given cross-flow plane. However, it is much more difficult for a model to capture the phase during which the end of a coherent structure passes through the cross-flow plane of interest and a new distribution of longitudinal vortices emerges. To decrease the frequency with which a reduced-order model must adjust to a new arrangement of near-wall longitudinal vortices, it is useful to utilize such models in a reference frame which convects at the average speed of the coherent structures.

The techniques of dynamical systems theory have encountered some success in analysing and interpreting turbulence dynamics (Aubry *et al.* 1988; Holmes, Lumley & Berkooz 1996). Due to their large range of spatial and temporal scales, however, turbulent flows are known to have relatively high dimensions in this framework even at fairly low Reynolds numbers, which makes analysis of these systems extremely difficult (Keefe, Moin & Kim 1992).

An example of one approach for determining reduced-order models is the ongoing work of anatomizing the coherent structures of wall-bounded turbulence using the proper orthogonal decomposition (POD) (Berkooz, Holmes & Lumley 1993). This decomposition provides a (numerically determined) set of modes which is particularly efficient in representing second-order turbulence statistics near a wall, at least when no control is applied to the flow. However, the equation expressing the evolution of and interaction between these modes is quite complex. The best way to extract POD modes for a controlled turbulent flow remains to be determined. Some sort of iterative technique, in which the control algorithm and the POD modes are sought simultaneously, might be required in order to extract a set of modes which efficiently captures the energetic structures actually present in the controlled flow. As the controlled flow is not statistically stationary, one might ultimately need a sequence of different POD models/control algorithms to completely relaminarize an initially turbulent flow, with the controller scheduling required based on an (evolving) bulk flow statistic such as total drag or turbulent kinetic energy.

As a preliminary example of control using such a reduced-order model, Coller, Holmes & Lumley (1994*a, b*) considers the control of a simple model problem (developed by Aubry *et al.* 1988) governed by a two-component equation with dynamics similar to that of a POD model of near-wall longitudinal vortices. This model equation is subjected to random excitation to account (albeit, roughly) for unmodelled system dynamics and disturbances. A strategy is developed and demonstrated which

delays heteroclinic transitions in this simple model as long as possible by sensing when the state is near an unstable fixed point and maintaining it there with feedback control for as long as possible. Once the state diverges from this fixed point, presumably due to the significant unmodelled dynamics of the flow (e.g. the passage of the head of a coherent structure), control is turned off until the state approaches the neighbourhood of another unstable fixed point. Such a ‘chaos control’ strategy is akin to that proposed by Ott, Grebogi & Yorke (1990) and implemented in a turbulent channel flow setting by Keefe (1993). Preliminary work on the application of this type of strategy to low Reynolds number turbulent flows is reviewed by Lumley & Blossey (1998). To date, approximately 20% drag reduction has been obtained with this approach in turbulent flows.

### 1.5. A need for model-based control strategies

The complex, multi-scale nature of turbulent flows has largely thwarted efforts to subdue turbulence with feedback based on either adaptive ‘black boxes’ or on physically based notions and has frustrated efforts to develop reduced-order models from which effective controls may be determined. We are thus driven to derive turbulence control algorithms directly from the equation known to govern the problem at hand. The rest of this paper describes and demonstrates one approach to determining such control strategies via optimal control theory and iterative direct numerical simulations.

## 2. Optimal and robust control in the predictive control framework

### 2.1. The seminal idea and an analogy to the game of chess

The general idea of the receding-horizon predictive control setting (as formulated in continuous time) is shown in figure 1. To put this approach into a more intuitive context, and to appreciate better the importance of the (somewhat mathematical) gradient-based optimization approach to the present problem, it is useful at the outset to compare and contrast the present approach to massively parallel brute-force algorithms recently developed to play the game of chess. The parallels and the shortcomings of this analogy highlight well the problem at hand.

The goal when playing chess is to capture the other player’s king through an alternating series of discrete moves with the opponent: at any particular turn, a player has to select one move out of at most thirty or so legal alternatives. Upon first inspection, this task seems quite simple compared to the problem of control of three-dimensional turbulence. Even once the problem is discretized in space and time, the turbulence control problem is generally a much higher-dimensional optimization problem, involving the coordination of a large array of actuators, where the effects of all control actions are intricately coupled via a high-dimensional, nonlinear, chaotic state governed by the Navier–Stokes equation.

To accomplish its optimization, a computer program designed to play the comparatively ‘simple’ game of chess, such as *Deep Blue* (Newborn 1997), must, in the worst case, plan ahead by iteratively examining a tree of possible evolutions of the game several moves into the future (Atkinson 1993)†. At each step, the program selects that move which leads to the best expected outcome, given that the opponent is doing the same, in the spirit of a non-cooperative game. The version of *Deep Blue* that defeated Garry Kasparov in 1997 was able to calculate up to 200 billion moves in the

† Note that extensive tables of opening sequences and endgame sequences are also stored in modern chess programs to assist with these phases of the game, though the bulk of the midgame must be examined essentially by brute force.

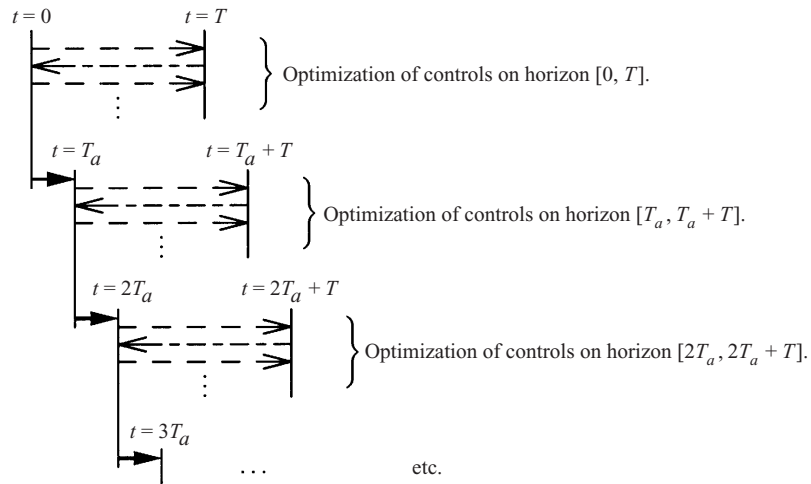


FIGURE 1. The sequence of events in receding-horizon predictive control. The heavy solid arrows indicate the flow advancement. The evolution of the ‘actual’ flow response to several ‘test’ distribution of controls is explored during the iterative flow prediction (dashed line) and adjoint computation (dot-dashed line) stages, during which the control is optimized by a gradient algorithm. Once this iteration converges, the flow is ‘advanced’ some portion  $T_a$  of the period  $T$  over which the control was optimized, and the optimization process is begun anew.

three minutes it was allowed to conduct each turn. Even with this extreme number of function evaluations at its disposal on this relatively simple problem, the algorithm was only about an even match with Kasparov’s human intuition.

A similar brute-force optimization strategy based on function evaluations alone might be suggested for the problem of turbulence control. In this context, so-called ‘genetic algorithms’ (Michalewicz 1996) are the primary candidates. The primary strengths of these algorithms are their ease of programming and their ability to minimize pathological functions in which gradient information is of limited usefulness. Such algorithms are effective for low-dimensional optimization problems, even in situations for which the evolution equation governing the system at hand is not available, so long as the number of parameters to be optimized is not very large (Padmanabhan, Bowman & Powell 1993; Koumoutsakos, Freund & Parekh 1998). They may also be viable in high-dimensional optimization problems when function evaluations can be performed extremely quickly (not the case with most DNS, but may be realized experimentally for statistically stationary optimization problems) and/or a very long time is given to conduct the optimization. In the case of the optimization (by biological adaptation) of the drag-reducing ribbed surface on the scales of fast-swimming sharks (see, e.g. Choi, Moin & Kim 1993 and Bechert *et al.* 1997), the optimization has taken, literally, millions of years. As the present optimization problem is very high-dimensional (up to  $O(10^7)$  control variables per optimization horizon) and function evaluations (direct numerical simulations) are very expensive, a more efficient optimization strategy is required.

An algorithm which is an improvement over the brute-force approach, suitable for optimizing the present problem in a reasonable amount of time, is available because

- (a) we know the equation governing the evolution of the present system, and
- (b) we can formulate the problem of interest as a functional to be minimized.

Taking these two facts together, we will devise and solve an iterative procedure based on gradient information, derived from an *adjoint field*, to optimize the controls for the

desired purpose on the prediction horizon of interest in an efficient manner. Only by exploiting such gradient information can the high-dimensional optimization problem at hand be made tractable. Note that it is desirable that the optimization problems we will formulate be constructed in such a manner that they are as well-conditioned (i.e. non-pathological) as possible in order to make them amenable to efficient gradient-based numerical optimization algorithms. To this end, several different formulations of the present control problem are discussed in §6.

It would seem that, in both the chess problem and the turbulence problem, the further into the future one can optimize the problem the better; however, both problems get exponentially harder to optimize as the prediction horizon is increased. Since only intermediate-term optimization is tractable, it is not always the best approach to represent the final objective in the cost functional. In the chess problem, though the final aim is to capture the other player's king, it is most effective to adopt a mid-game strategy of establishing good board position and achieving material advantage. Similarly, if the turbulence control objective is reducing drag, it is found (see §7) that it is most effective along the way to minimize a finite-horizon cost functional related to the turbulent kinetic energy of the flow, since the turbulent transport of momentum is responsible for inducing a substantial portion of the drag in a turbulent flow. In a sense, turbulence is the 'cause' and high drag is the 'effect', and it is most effective to target the 'cause' in the cost functional when optimizations on only intermediate prediction horizons are possible.

In addition, a smart optimization algorithm allows excursions in the short term if such a strategy leads to a long-term advantage. For example, in chess, a good player is willing to sacrifice a lesser piece if, by so doing, a commanding board position is attained and/or a restoring exchange is forced a few moves later. Similarly, by allowing a turbulence control scheme to increase (temporarily) the turbulent kinetic energy of a flow, a transient may ensue which, eventually, effectively diminishes the strength of the near-wall coherent structures. It is shown in §7 that terminal control strategies, aimed at minimizing the turbulence only at the end of each optimization period, appear to have an advantage over regulation strategies, which penalize excursions of the turbulent kinetic energy over the entire prediction horizon.

## 2.2. Related approaches

The use of adjoint-based techniques to optimize controls for nonlinear systems in the receding-horizon predictive control framework is well developed for both continuous-time and discrete-time problem formulations. References on these topics include: Bryson & Ho (1975), Garci, Prett & Morari (1989), Mayne & Michalska (1990), Soeterboek (1992), Clarke (1994), Muske & Edgar (1997), and Sutton & Bitmead (1999). These techniques are related to those used in (essentially time-invariant) distributed optimization problems, such as the optimization of bioartificial arteries (Petzold *et al.* 1997), the prediction of bone hardening due to applied periodic loading (Jacobs *et al.* 1997), and the optimization of airfoils for aerodynamic design (Reuther *et al.* 1996).

In the active feedback control setting, the predictive control technique has found broad application and popular acceptance in applications for which the system of interest evolves but slowly, such as in the chemical process industry (Seborg, Edgar & Mellichamp 1989). In such applications, the system evolves so slowly that it may be considered as 'frozen' in time, and a fast computer may be used to predict the evolution of the system many times to determine iteratively the most suitable set of controls to apply to the system over the given time horizon  $T$ . As mentioned earlier,

given that the governing equation is known and a mathematical statement of the control problem is available, it is a straightforward exercise to determine gradient information with which the controls may be efficiently updated. The predictive control approach is useful, for example, for determining a schedule of controls to switch effectively from one set point in a chemical process to another, while keeping rise time, overshoot, and settling time to a minimum. The predictive control approach is very versatile, and is effective in otherwise problematical systems, including those which are inherently nonlinear, those which contain saturation constraints and rate constraints on the actuators, and those which are characterized by significant time delays between application of the control and measurement of its effects (see, e.g. Yang & Polak 1993).

Note that the present approach is sometimes referred to as Model Predictive Control (MPC) in the controls literature. The ‘model’ of the fluid flow used in the present work is direct numerical simulation, which is essentially an exact evolution of the Navier–Stokes equation governing the system of interest. As the word ‘model’ in the fluids literature generally has the connotation of an *approximate* model, we have, for clarity, chosen to drop the word ‘model’ from our description of the present approach.

### 2.3. Predictive control optimization in the fluid mechanical setting

Turbulent flows, by most measures, are not slowly-evolving systems. In a practical implementation, it is usually impossible to predict iteratively several possible evolutions of a turbulent flow (resulting from several possible sequences of control application) during a period of time short enough that the actual flow may be considered as ‘frozen’ in time. Thus, it is impossible to implement the predictive control algorithm directly in a practical setting for the problem of turbulence. However, we can perform such a procedure in a computer, where a turbulent flow may be (artificially) ‘frozen’ in time. Such an exercise is not considered as simply an abstract *Gedankenexperiment*, as it allows us to determine the system performance possible given a certain class of flow actuation and qualify how optimized controls correlate with the near-wall coherent structures believed to dominate the process of turbulence production in wall-bounded flows. Further, various approaches have been proposed to distil practical feedback schemes from the predictive control approach, as discussed in §2.4. The present exercise is a necessary step in the development of such optimization algorithms for practical feedback control rules.

The mathematical details of optimal control theory applied to the Navier–Stokes equation and other nonlinear PDEs have a long and rich history which will not be expounded here. Significant early advances in this area are well documented by Morse & Feshbach (1953), Lions (1968), and Finlayson (1972). After something of a hiatus in this area, there has been a resurgence of interest in the mathematical properties of these approaches, such as existence and uniqueness of solutions and proofs of convergence of proposed numerical algorithms. Abergel & Temam (1990), Gunzburger, Hou & Svobodny (1990), Sritharan (1991, 1998), Gunzburger (1995), Lagnese, Russell & White (1995), Fursikov, Gunzburger & Hou (1998), and Bewley *et al.* (2000) discuss several of these recent advances.

Early attempts to implement predictive control with adjoint-based optimization approaches compromised on the length of the prediction horizon, taking  $T^+ \lesssim 1$  (Bewley *et al.* 1993; Hill 1993; Lee, Kim & Choi 1998; etc.). This approach has the dubious distinction of being dubbed the ‘suboptimal approximation’. The main reason for making such an assumption is that it results in control rules which are easy

to implement and solve, eliminating the tedious and impractical predictive control framework. Another advantage of this approach is that, by approximating the nonlinear terms with a Taylor series expansion of wall information (Hill 1993) or neglecting the nonlinear terms altogether (Lee *et al.* 1998), the resulting problem can be solved analytically, resulting in a control scheme in terms of wall information only. Though schemes of this ‘suboptimal’ variety do give drag reductions in the neighbourhood of 20% (Bewley *et al.* 1993; Hill 1993; Lee *et al.* 1998), this approach is recognized to neglect the nonlinear evolution central to the development of turbulent flows. The importance of using intermediate prediction horizons which at least partially capture the evolution of the near-wall coherent structures is now readily apparent (see §7).

#### 2.4. Adjoint-based ensemble optimization of practical control algorithms – a preview

The present work is a first step towards developing finite-horizon, adjoint-based techniques for the optimization of practical feedback control rules for turbulent flows of the two types illustrated in figure 2. The (initially undetermined) coefficients of the feedback rules in both configurations may be optimized rigorously with predictive approaches based on the adjoint analysis developed here (Bewley, Moin & Temam 1996). In this approach, an identical control rule is applied to large ensembles (thousands) of control points on the walls of a representative turbulent flow (as the flow considered is statistically homogeneous in the streamwise and spanwise directions, this approach is reasonable). The gradient information determined by the adjoint approach is then used to determine the sensitivity of the cost functional to modification of the coefficients in this control rule (rather than modification of the control distribution itself). If the ensemble is large enough with respect to the complexity of the control rule being optimized, optimization via this approach should lead to a set of coefficients which generalizes well to other turbulent flow realizations with similar near-wall dynamics.

In the output feedback configuration, the flow is controlled using computationally inexpensive direct feedback from instantaneous flow measurements. Note that the structure of this feedback rule may be nonlinear and may incorporate a finite impulse response (FIR) filter to account for information from past measurements in the control rule.

In the estimator-based configuration, the filter used effectively establishes a time-evolving estimate of the flow state near the wall, assimilating appropriately the information contained in the available sequence of (noisy) flow measurements. The model used in the estimator may in fact be the full Navier–Stokes equation or (preferably) a reduced-order representation thereof, as discussed earlier. The flow is then controlled with a (possibly nonlinear) control rule based on this flow estimate. It is important that the system model used in the estimator should at least roughly model the nonlinear dynamics of the full flow system (Bewley 1999).

In the linear case, the estimation problem and the control problem are linked only when they are optimized in the non-cooperative game framework of ‘robust control’, in which a finite component of ‘worst case’ noise is introduced which is maximally detrimental to the control objective (Green & Limebeer 1995). Such an approach is well developed for linear problems, and is referred to as  $\mathcal{H}_\infty$  control. Doyle *et al.* (1989) present a compact form of this approach which makes it straightforward to apply to linear problems, as illustrated in Bewley & Liu (1998) for the control of the linear stages of transition. This non-cooperative game framework, which (albeit in the brute-force context) is essential to the success of the chess algorithm (which is, in

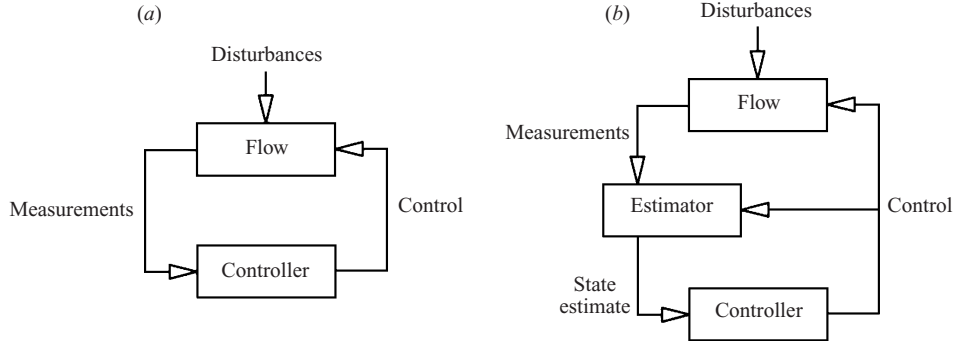


FIGURE 2. Examples of practical feedback control configurations based on limited noisy flow measurements. The unknown feedback coefficients in both configurations may be optimized numerically with the techniques based on the optimization approach developed in this paper. (a) Output feedback configuration, (b) estimator-based configuration.

fact, a non-cooperative game), is also useful in the present problem. As discussed in detail in Bewley & Liu (1998), this framework allows feedback gains to be kept to a minimum for components of the system not relevant to the control problem at hand. These reduced feedback gains result in reduced opportunity for improper feedback to disrupt the closed-loop system.

New methods of applying the robust approach to distributed, fully nonlinear systems such as turbulence have also been mathematically investigated (Bewley *et al.* 2000). It appears likely that the robust aspect of the non-cooperative optimization framework will be key to the effective implementation of feedback control of turbulence when only limited noisy measurements are available.

### 3. Governing equation

The problem we consider in the present paper is the control of a fully developed turbulent channel flow with full flowfield information available to the control algorithm. The flow is governed by the incompressible Navier–Stokes equation inside a three-dimensional rectangular domain  $\Omega$  with unsteady wall-normal velocity boundary conditions  $\phi$  applied on the walls  $\Gamma_2^\pm$  as the control, as depicted in figure 3. The extent of the computational domain is chosen to be large enough in the homogeneous directions ( $x_1$  and  $x_3$ ) that the convenient (though non-physical) periodic boundary conditions applied in these directions have minimal effect on the nature of the near-wall turbulence. This is illustrated qualitatively in figure 4 in §5 and quantitatively (by the decay of the spatial correlations of the turbulence to zero well before the edge of the computational domain) in plots such as those represented in figures 5(a) and 6(a). Though this is an idealized geometry, it gives insight into the nature of near-wall turbulence which can later be exploited in more practical configurations, such as the control of a spatially developing boundary layer with discrete wall-mounted actuators.

Three vector fields are first defined: the flow state  $\mathbf{q}$ , the flow perturbation state  $\mathbf{q}'$ , and the adjoint state  $\mathbf{q}^*$ :

$$\mathbf{q}(\mathbf{x}, t) = \begin{pmatrix} p(\mathbf{x}, t) \\ \mathbf{u}(\mathbf{x}, t) \end{pmatrix}, \quad \mathbf{q}'(\mathbf{x}, t) = \begin{pmatrix} p'(\mathbf{x}, t) \\ \mathbf{u}'(\mathbf{x}, t) \end{pmatrix}, \quad \mathbf{q}^*(\mathbf{x}, t) = \begin{pmatrix} p^*(\mathbf{x}, t) \\ \mathbf{u}^*(\mathbf{x}, t) \end{pmatrix}.$$

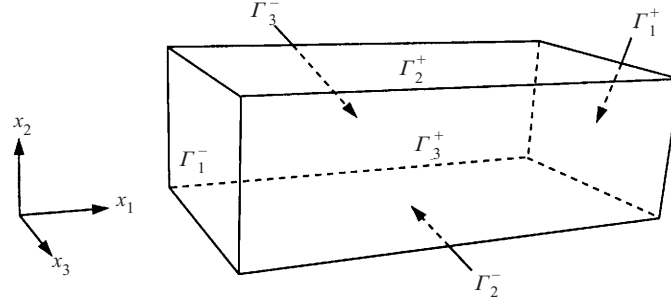


FIGURE 3. Channel flow geometry. The interior of the domain is denoted  $\Omega$  and the boundaries of the domain in the  $x_i$ -direction are denoted  $\Gamma_i^\pm$ . Unsteady wall-normal velocity boundary conditions are applied on the walls  $\Gamma_2^\pm$  as the control, with periodic boundary conditions applied in the streamwise direction  $x_1$  and spanwise direction  $x_3$ .

Each of these vector fields is composed of a pressure component and a velocity component, all of which are continuous functions of space,  $\mathbf{x}$ , and time,  $t$ . The velocity components themselves are also vectors, with components in the streamwise direction  $x_1$ , the wall-normal direction  $x_2$ , and the spanwise direction  $x_3$ . Partial differential equations governing all three of these fields will be derived in due course, and the motivation for introducing  $\mathbf{q}'$  and  $\mathbf{q}^*$  will be given as the need for these fields arises in the control derivation. Only after the control problem has been derived completely in differential form is it discretized in space and time. For the current three-dimensional nonlinear problem (which necessitates a mixture of implicit and multi-step explicit schemes for accurate time advancement, with incompressibility enforced by an involved fractional step algorithm), this approach (referred to as ‘optimize then discretize’) is found to yield adjoint systems which are the easiest to understand and to code. For simpler systems, such as the one-dimensional linear problem of transition control examined in Bewley & Liu (1998), the discrete control expressions derived from the discrete form of the governing equation are found to be tractable (a setting referred to as ‘discretize then optimize’). Note that the processes of optimization and discretization, in general, do not commute, and thus these two approaches are not necessarily equivalent even upon refinement of the space/time grid (Vogel & Wade 1995).

The governing equation may be written functionally as

$$\mathcal{N}(\mathbf{q}) = \begin{pmatrix} 0 \\ -\mathbf{r}P_x(\mathbf{x}, t) \end{pmatrix} \quad \text{in } \Omega, \quad (3.1a)$$

where  $\mathcal{N}(\mathbf{q})$  is defined below in (3.3) and  $\mathbf{r}$  is a unit vector in the  $x_1$ -direction. An external pressure gradient  $P_x$  is applied to induce a mean flow in the  $x_1$ -direction. The boundary conditions on the state  $\mathbf{q}$  are assumed to be periodic in the streamwise and spanwise directions (for computational simplicity), and a wall-normal control velocity is distributed over the walls such that

$$\mathbf{u} = -\phi \mathbf{n} \quad \text{on } \Gamma_2^\pm, \quad (3.1b)$$

where  $\mathbf{n}$  is the unit outward normal to the boundary  $\partial\Omega$ . Initial conditions on the velocity are prescribed such that

$$\mathbf{u} = \mathbf{u}_0 \quad \text{at } t = 0. \quad (3.1c)$$

The flow is sustained by an externally applied<sup>†</sup> mean pressure gradient (per unit mass)  $P_x$  in the streamwise direction; this mean pressure gradient may be either a fixed constant or modified at each time step in order to maintain a constant mass flux through the channel. The control  $\phi$  is constrained to inject zero net mass at the walls, such that

$$\int_{\Gamma_2^+} \phi \, d\mathbf{x} = \int_{\Gamma_2^-} \phi \, d\mathbf{x} = 0 \quad \forall t. \quad (3.2)$$

Note that boundary conditions and initial conditions on the pressure  $p$  are not needed for a well-posed problem formulation. Mathematically speaking (Temam 1984; Abergel & Temam 1990; Bewley *et al.* 2000), the control derivation presented in this paper may be conducted on a divergence-free submanifold of  $(L^2(\Omega))^3$ , in which the pressure has been removed from the governing equation using the Leray–Helmholtz formulation of the Navier–Stokes equation. This ‘abstract form’ of the incompressible Navier–Stokes equation facilitates mathematical analysis. In the present paper, however, we will retain the pressure in our derivations; this more intuitive form both eases the treatment of inhomogeneous boundary conditions and facilitates the direct extension of the present analysis to compressible flows, as discussed in Appendix B.

For clarity, all differential equations are written in operator form in this discussion, with these operators defined when first introduced. The (nonlinear) Navier–Stokes operator for the present case, in which the flow is assumed to have uniform density and viscosity, is given by

$$\mathcal{N}(\mathbf{q}) = \left( \begin{array}{c} \frac{\partial u_j}{\partial x_j} \\ \frac{\partial u_i}{\partial t} + \frac{\partial u_j u_i}{\partial x_j} - \nu \frac{\partial^2 u_i}{\partial x_j^2} + \frac{\partial p}{\partial x_i} \end{array} \right). \quad (3.3)$$

Note that  $p$  is the pressure divided by the density and  $\nu$  is the kinematic viscosity. Define also  $\bar{\tau}_w/\rho \triangleq -\nu \partial \bar{u}_1 / \partial n|_{\Gamma_2^\pm}$  as the mean skin friction on the wall for the uncontrolled turbulent channel flow divided by the density (averaged in space and time),  $u_\tau \triangleq (\bar{\tau}_w/\rho)^{1/2}$  as the mean friction velocity,  $\delta$  as the channel half-width, and  $Re_\tau \triangleq u_\tau \delta / \nu$  as the Reynolds number based on the mean friction velocity and the channel half-width. The flows considered in this work are constant mass flux flows at  $Re_\tau = 100$  and  $Re_\tau = 180$ . (This corresponds to Reynolds numbers based on the mean centreline velocity of the uncontrolled flow,  $Re_c = u_c \delta / \nu$ , of  $Re_c = 1712$  and  $Re_c = 3247$ , and to Reynolds numbers based on the bulk velocity,  $Re_B = u_B \delta / \nu$ , of  $Re_B = 1429$  and  $Re_B = 2797$ .) All velocities are normalized by the friction velocity  $u_\tau$ , and therefore may also be marked with a + superscript. All lengths are normalized by  $\delta$  unless marked with a + superscript, in which case they are normalized by the wall unit  $\nu/u_\tau$ . All times are normalized by  $\delta/u_\tau$  unless marked with a + superscript, in which case they are normalized by  $\nu/u_\tau^2$ . Note that, with this normalization,  $\nu = 1/Re_\tau$  in the above equation for  $\mathcal{N}(\mathbf{q})$ .

<sup>†</sup> By this, we mean that the mean pressure gradient is a quantity which is considered as constant when computing the adjoint field  $\mathbf{q}^*$  and the gradient  $\mathcal{D}\mathcal{J}/\mathcal{D}\phi$ . The opposite viewpoint may also be taken in this framework; namely, the mean pressure gradient may be taken as a (scalar) variable and included together with the distributed field variable  $\mathbf{q}$  in the optimization process. In this framework, an integral constant mass flux constraint is included together with the PDE governing the system (the Navier–Stokes equation) in the governing equation set. This formulation is a bit more cumbersome and leads to essentially the same results.

#### 4. Numerical method

The control formulations discussed in §2 (and to be presented in greater detail in §6) were tested in direct numerical simulations of constant mass flux, fully developed turbulent channel flows at both  $Re_\tau = 100$  and  $Re_\tau = 180$ . The coarse-grid, inexpensive lower Reynolds number simulations were used to perform parametric studies to determine the appropriate range of parameters to test more accurately on a finer grid at the higher Reynolds number. In the present work, Fourier transform techniques are used to compute spatial derivatives in the homogeneous directions with 3/2 dealiasing of the nonlinear terms, and an exactly energy-conserving second-order finite difference scheme is used to compute spatial derivatives on the stretched grid in the wall-normal direction. Very fine grid resolution is required near the wall to resolve the shear layer; the mesh is fairly fine even up to the centre of the domain because the second-order difference scheme used to compute the derivatives in this direction is numerically dispersive. The computational grid is staggered in the wall-normal direction to prevent decoupling of the even and odd modes of the pressure.

A substantially different numerical method was needed in the present computations than was used in, for example, the fully spectral code of Kim, Moin & Moser (1987), in order to best facilitate implementation of the wall-normal velocity boundary conditions. The flow is advanced in time using an explicit low-storage third-order Runge–Kutta method for all terms involving  $x_1$ - and  $x_3$ -derivatives and an implicit Crank–Nicholson method at each Runge–Kutta substep for all terms involving  $x_2$ -derivatives, with a method based on that of Akselvoll & Moin (1995). A temporal discretization implicit in the  $x_2$ -derivatives is necessary to mitigate the CFL time step restriction when control is applied, as the control fluid at the wall is directed in the  $x_2$ -direction, which is precisely the region and direction in which the mesh must be refined most to resolve the shear layer. Unfortunately, this implicit time advancement necessitated the use of a finite-difference scheme in the wall-normal direction rather than the (more accurate) Chebyshev approach.

For the  $Re_\tau = 180$  simulations, the number of Fourier modes used<sup>†</sup> is  $170 \times 129 \times 170$  in the  $x_1$ -,  $x_2$ - and  $x_3$ -directions respectively (i.e.  $256 \times 129 \times 256$  dealiased collocation points), and the size of the computational domain in wall units is  $L_1^+ = 2260$ ,  $L_2^+ = 360$ ,  $L_3^+ = 1130$ . The resulting effective grid resolution in the streamwise and spanwise directions (on collocation points determined without the extra 3/2 padding) is  $\Delta x_1^+ = 13$ ,  $\Delta x_3^+ = 7$ . Hyperbolic tangent stretching of the grid is used in the wall-normal direction, resulting in a grid spacing of  $\Delta x_2^+ = 0.6$  adjacent to the wall and  $\Delta x_2^+ = 5.2$  in the centre of the channel.

For the  $Re_\tau = 100$  simulations, the number of Fourier modes used<sup>†</sup> is  $42 \times 65 \times 42$  (i.e.  $64 \times 65 \times 64$  dealiased collocation points), and the size of the computational domain is  $L_1^+ = 1260$ ,  $L_2^+ = 200$ ,  $L_3^+ = 420$ . The resulting effective grid resolution in the streamwise and spanwise directions is  $\Delta x_1^+ = 30$ ,  $\Delta x_3^+ = 10$ . The wall-normal grid spacing is  $\Delta x_2^+ = 0.7$  adjacent to the wall and  $\Delta x_2^+ = 5.8$  in the centre of the channel.

#### 5. Dynamics and statistics of uncontrolled system

The nature of a turbulent flow is characterized well by observing the fluid at various points throughout the channel in a reference frame which moves with the

<sup>†</sup> The number of modes used in the homogeneous directions for the fast Fourier transforms (FFTs), which is expanded by a factor of 3/2 to dealias the nonlinear terms, is an even power of two, which results in maximum efficiency of the FFT routines.

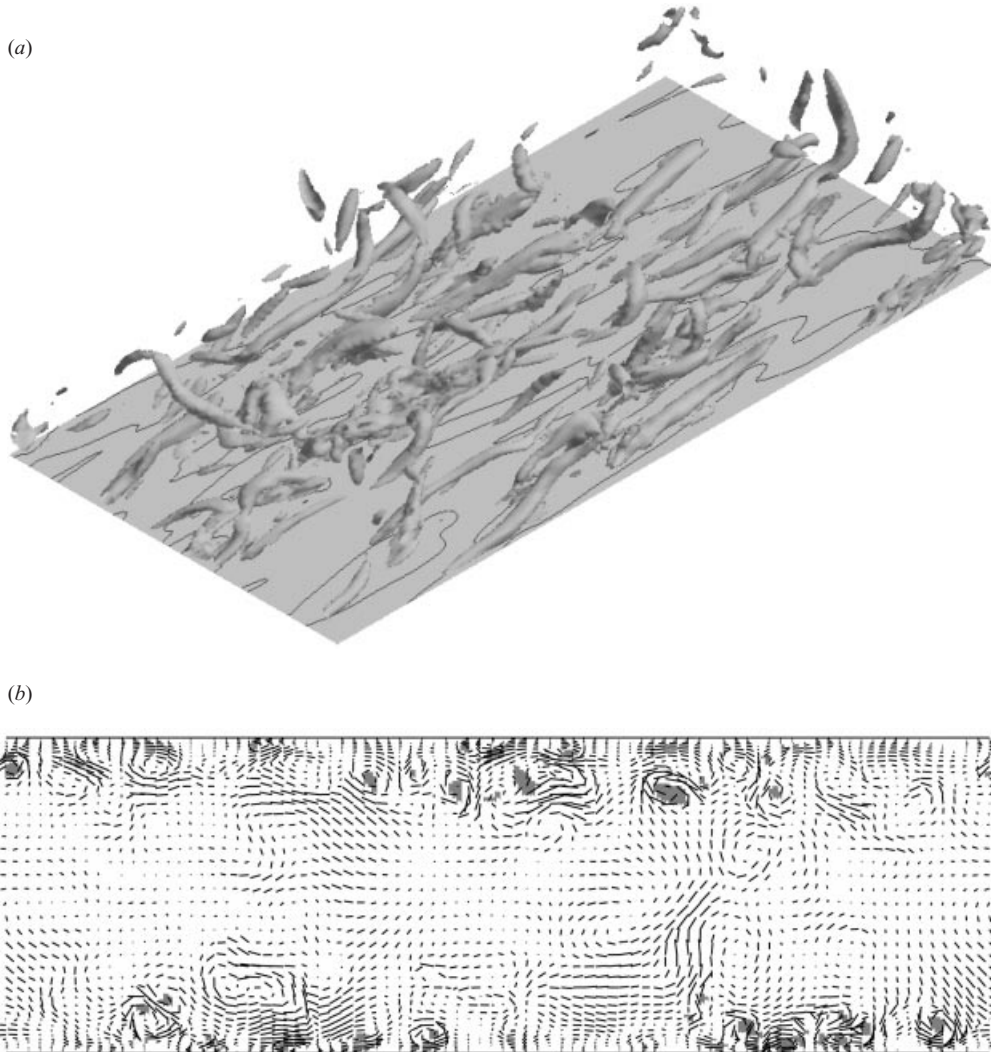


FIGURE 4. Fully developed turbulent channel flow realization at  $Re_\tau = 180$ , no control. Regions of the flow with positive discriminant  $D > D_{\text{threshold}}$  are shaded, indicating fluid motion which, in a pointwise sense, is vortical in nature. In the three-dimensional visualization (a), the flow is from lower left to upper right and, for clarity, only one quarter of the lower half of the domain  $\Omega$  used in the computations (see figure 3) is shown. In the crossflow visualization (b), for clarity, the crossflow velocity vectors (indicated by the arrows) are marked on only one ninth of the gridpoints used in the computations in this crossflow plane.

local velocity. In this reference frame, the point under consideration is a critical point, as the local streamline slope is indeterminate. Thus, a critical point analysis of the type discussed by Perry & Chong (1987), Chong, Perry & Cantwell (1990), and Blackburn, Mansour & Cantwell (1996) is appropriate. A single scalar quantity  $D$ , the discriminant of the velocity gradient tensor, provides a useful identification of regions in the flow which, in this context, are ‘focus’ in nature. Such focus regions roughly correspond to ‘vortex-type’ regions in a turbulent flowfield, though this description is only pointwise in nature.

The velocity gradient tensor discussed in this work is defined in wall units  $A_{ij} \triangleq$

$\partial u_i^+ / \partial x_j^+$ . The second and third invariants of  $\mathbf{A}$  are  $Q \triangleq \{[\text{tr}(\mathbf{A})]^2 - \text{tr}(\mathbf{A}^2)\}/2$  and  $R \triangleq -\det(\mathbf{A})$ . The discriminant of the velocity gradient tensor is given by  $D = (27/4)R^2 + Q^3$ . Regions with  $D > 0$  are characterized by a velocity gradient tensor with one real and two complex eigenvalues (and thus a swirling, vortex-type motion in the Lagrangian reference frame discussed above), whereas regions with  $D \leq 0$  are characterized by three real eigenvalues. As illustrated in figure 4, visualizations of isosurfaces of the discriminant of the velocity gradient tensor provide a handy identification technique for the location of ‘vortex-type’ motions in the turbulent flow. For clarity, the visualizations of the discriminant presented in this work identify only regions of positive discriminant greater than a small threshold value  $D > D_{\text{threshold}}$ , where  $D_{\text{threshold}} = 10^{-5}$ .

As direct numerical simulations produce a tremendous amount of data, it is important to analyse relevant statistics of the flowfields they generate, in addition to the instantaneous visualizations, in order to understand better the phenomena taking place in a quantitative sense and how these integral measures of the turbulence are modified by the application of control. Gross flowfield statistics useful for monitoring the time evolution of the flow include the total drag and the turbulent kinetic energy (TKE). The statistics used in the present work to examine the variation of the turbulence with distance from the wall  $x_2$  are the mean velocity  $\bar{u}_1$ , the root-mean-square velocity fluctuations  $u_{i,rms}$ , the Reynolds stress  $-\bar{u}_1\bar{u}_2$ , the total stress  $-\bar{u}_1\bar{u}_2 + \nu \partial \bar{u}_1 / \partial x_2$ , and the two-point correlations  $R_{ij}(\mathbf{r}) \triangleq \overline{u_i(\mathbf{x})u_j(\mathbf{x} + \mathbf{r})}$  and their Fourier transform, the spectra  $E_{ij}(\mathbf{k})$ . Note that the overbar implies averages in the homogeneous directions  $x_1$  and  $x_3$  and, when the flow is statistically stationary, in time. At times we will distinguish the fluctuating component of the flow  $\mathbf{v}$  separately from the mean component  $\bar{\mathbf{u}}$  such that  $\mathbf{u} = \bar{\mathbf{u}} + \mathbf{v}$ . Further discussion of these statistics and their behaviour in uncontrolled turbulent channel at  $Re_\tau = 180$  may be found in Kim *et al.* (1987). Selected statistics from the present computations at  $Re_\tau = 100$  and  $Re_\tau = 180$  are shown in figures 5 and 6. Quantitative comparison of the  $Re_\tau = 180$  statistics reported in figure 6 with the benchmark computations of Kim *et al.* (1987) indicate that the numerical method used in the present computations is sufficiently accurate.

## 6. Application of optimal control theory to incompressible turbulence

The present section briefly derives the control approach used, without getting into the mathematics regarding the rigorous proofs of existence and uniqueness of the solution to the control problem or the convergence of the numerical algorithm. The notation is adapted from Abergel & Temam (1990) and Bewley *et al.* (2000), to which readers are referred for discussions regarding these mathematical issues and the generalization to the robust control (i.e. non-cooperative game) setting.

### 6.1. Statement of physical problem: definition of cost functional

The optimal control problem is akin to a problem of economics; the first step in solving it is to represent the problem of interest as a cost functional,  $\mathcal{J}(\phi)$ , to be minimized<sup>†</sup>. The performance of the control algorithm for this type of problem is

<sup>†</sup> In the approach taken here, the state equation is, effectively, taken into account in the cost functional  $\mathcal{J}(\phi)$ , and the minimization is performed with respect to the control variable  $\phi$  alone. Another approach, sometimes referred to as the ‘all at once’ approach, is to write the cost functional as  $\mathcal{J}(\mathbf{u}, \phi)$  and to write the state equation separately, applying this equation as a feasibility constraint on the state  $\mathbf{u}$  rather than incorporating it when computing the gradient of the cost functional (Heinkenschloss 1997). The former approach appears to be more easily managed numerically in systems with very large state dimension.

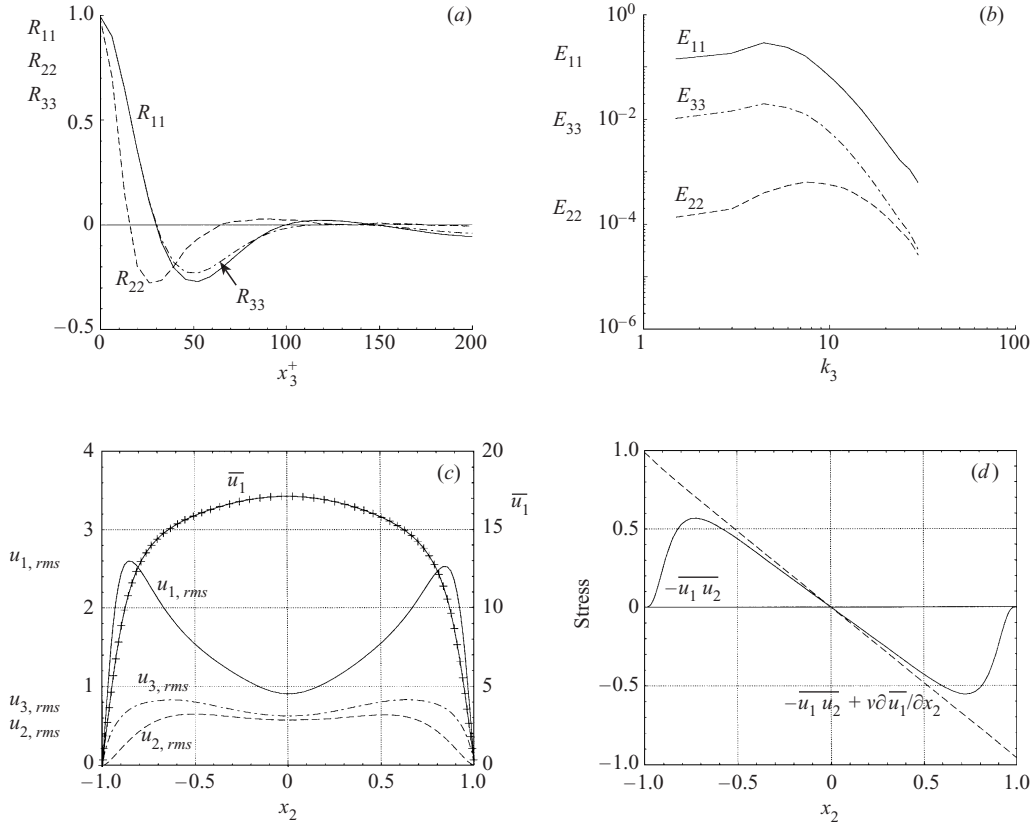


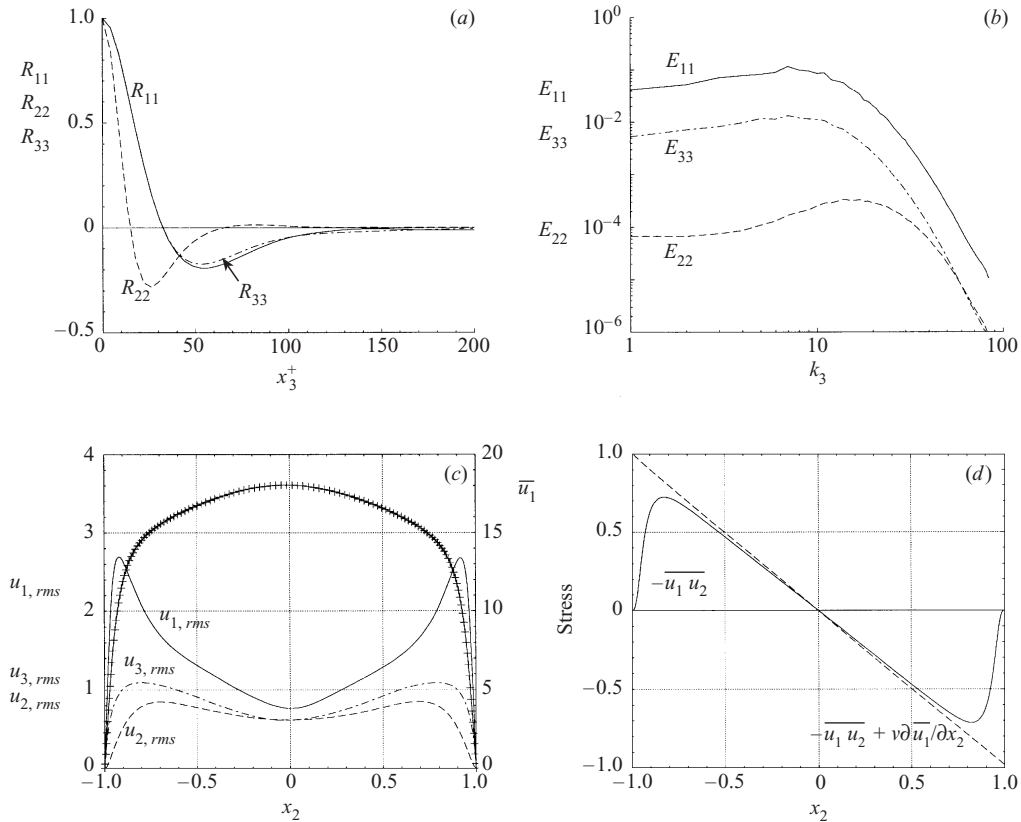
FIGURE 5. Selected time-averaged statistics of the uncontrolled turbulent channel flow at  $Re_\tau = 100$ : (a) spanwise two-point correlations at  $x_2^+ = 5.4$ ; (b) spanwise one-dimensional energy spectra at  $x_2^+ = 5.4$ ; (c) profiles of r.m.s. velocity fluctuations (left-hand scale) and mean velocity (right-hand scale); (d) profiles of Reynolds stress (—) and total stress (-----).

quite sensitive to the cost functional definition, and thus this topic warrants a detailed analysis in the context of the flow physics under consideration. In the present problem, control  $\phi$  is to be applied to minimize the drag averaged over a representative wall section and a long time horizon using the least amount of control effort possible. At present, it appears as if optimization of the nonlinear Navier–Stokes control problem over an infinite time horizon, which would require the solution of a very difficult Hamilton–Jacobi–Bellman (HJB) problem in infinite dimension (Sriharan 1991), is computationally intractable. However, optimizations on intermediate time horizons (i.e.  $T^+ \approx O(25)$ ) certainly are tractable. Thus, we must choose at the outset a ‘design’ time horizon over which we will determine controls which optimize the given objective; without loss of generality, let us consider the optimization horizon  $(0, T)$ .

#### Case (a): minimization of drag

A relevant cost functional for the minimization of drag on the walls  $\Gamma_2^\pm$  and over the horizon  $(0, T)$  with finite control effort is

$$\mathcal{J}_{\text{DRAG}}(\phi) = -d_1 \int_0^T \int_{\Gamma_2^\pm} v \frac{\partial u_1(\phi)}{\partial n} \, d\mathbf{x} \, dt + \frac{\ell^2}{2} \int_0^T \int_{\Gamma_2^\pm} \phi^2 \, d\mathbf{x} \, dt.$$

FIGURE 6. As figure 5 but at  $Re_\tau = 180$ .

The first term is a measure of exactly that quantity we would like to minimize<sup>†</sup>: in this case, the drag due to skin friction (note that the negative sign is needed because  $\partial/\partial n \triangleq \mathbf{n} \cdot \nabla$ , where  $\mathbf{n}$  is defined as an *outward* facing normal). The second term is a measure of the magnitude of the control. These quantities are integrated over the wall section and time period under consideration and weighted together with a factor  $\ell^2$ , which represents the price of the control. This quantity is small if the control is ‘cheap’ (which reduces the significance of the latter term and generally results in greater control effort), and large if applying control is ‘expensive’.

Dimensional constants  $d_i$ , which are the appropriate functions of the kinematic viscosity  $\nu$ , the channel half-width  $\delta$ , and the friction velocity  $u_\tau$ , are included in all cost functionals we will consider simply to make them dimensionally consistent.

#### Case (b): regulation of turbulent kinetic energy

As only an intermediate value of  $T$  can be afforded, minimization of a cost functional representing exactly the quantity of interest (drag) is not necessarily the most effective means of reducing the quantity of interest over the long term (as  $t \rightarrow \infty$ ). As discussed earlier, turbulence causes wall-normal convective transport

<sup>†</sup> Note that the drag reduction problem is a minimization problem, not a regulation problem; solutions in which the first term of  $\mathcal{J}_{\text{DRAG}}$  are negative, if they exist, are preferred over those in which this term is zero. It is shown in Bewley *et al.* (2000) that posing this type of cost functional (linear in the flow variable rather than quadratic in the flow variable) in no way hampers the proofs of existence and uniqueness of the solution of the control problem.

in the near-wall region which, in turn, increases the drag, heat transport, and scalar mixing in the flow. It is thus reasonable for the cost functional to target the turbulence (the ‘cause’) over each finite optimization horizon rather than the drag increase due to the turbulence (the ‘effect’). More precisely, such a cost functional might target the time-averaged value of the turbulent kinetic energy (TKE); a relevant cost functional for this formulation is†

$$\mathcal{J}_{\text{TKE}(\text{reg})}(\phi) = \frac{d_2}{2} \int_0^T \int_{\Omega} |\mathbf{u}(\phi)|^2 \, d\mathbf{x} \, dt + \frac{\ell^2}{2} \int_0^T \int_{\Gamma_{\pm}^{\pm}} \phi^2 \, d\mathbf{x} \, dt.$$

*Case (c): regulation of enstrophy*

Among mathematical audiences, regulation of the square of the vorticity (i.e. the enstrophy) is sometimes preferred over the regulation of the turbulent kinetic energy. This preference is well-founded mathematically, as:

1. The Poincaré inequality implies that regulation of enstrophy (or the  $H^1$ -norm of the turbulent field) directly results in regulation of turbulent kinetic energy (the  $L^2$ -norm of the turbulent field). Mathematically speaking, in a continuous formulation, the converse is not necessarily true (though, once discretized, the two norms are ‘equivalent’ up to a very large constant).

2. The Sobolev inequalities used for bounding the influence of the nonlinear term on a system governed by the Navier–Stokes equation are related to the  $H^1$ -norm of the turbulent field.

The cost functional appropriate for enstrophy regulation is

$$\mathcal{J}_{\text{ENS}(\text{reg})}(\phi) = \frac{d_3}{2} \int_0^T \int_{\Omega} |\nabla \times \mathbf{u}(\phi)|^2 \, d\mathbf{x} \, dt + \frac{\ell^2}{2} \int_0^T \int_{\Gamma_{\pm}^{\pm}} \phi^2 \, d\mathbf{x} \, dt.$$

For the special case of locally isotropic turbulence, there is a particularly simple relationship between the one-dimensional energy spectra and the one-dimensional enstrophy spectra, as shown in figure 7.

On physical grounds, it may be argued that controlling the turbulent kinetic energy is more effective than controlling the enstrophy. The explanation for this, at least in homogeneous isotropic turbulence, is classical (see figure 7): the low wavenumbers of turbulence generally feed the high wavenumbers, where the turbulent kinetic energy is effectively dissipated by viscosity. In this well-known ‘turbulent cascade’, it is the low wavenumbers that acquire the turbulent kinetic energy from the energy of the mean flow, and thus it is those which should be targeted by the cost functional. Using enstrophy in the cost functional, however, effectively weights the high wavenumbers of the turbulence spectrum by a factor of  $k^2$ . Further, the turbulent cascade of energy from the low wavenumbers to the high wavenumbers takes a finite amount of time which may not be small with respect to the optimization horizons  $T^+$  which can be afforded in the simulations. Thus, for intermediate optimization horizons,  $T^+ \approx O(25)$ , perhaps one may identify the large spatial scales of the turbulence as the ‘cause’ of the phenomena of interest and therefore favour cost functionals which emphasize those. In addition, formulations derived from enstrophy-based cost functionals, which focus on the turbulence at the dissipation scales, require much

† Note that, strictly speaking,  $\mathcal{J}_{\text{TKE}(\text{reg})}(\phi)$  is influenced both by the turbulent kinetic energy  $\int_0^T \int_{\Omega} |\mathbf{v}(\phi)|^2 \, d\mathbf{x} \, dt$  and the effect of the mean field,  $\int_0^T \int_{\Omega} |\bar{\mathbf{u}}(\phi)|^2 \, d\mathbf{x} \, dt$ . It was found in the present study (apparently due to the zero-mass-flux constraint (3.2) that formulations based on  $\int_0^T \int_{\Omega} |\mathbf{v}(\phi)|^2 \, d\mathbf{x} \, dt$  and those based on  $\int_0^T \int_{\Omega} |\mathbf{u}(\phi)|^2 \, d\mathbf{x} \, dt$  give essentially identical results.

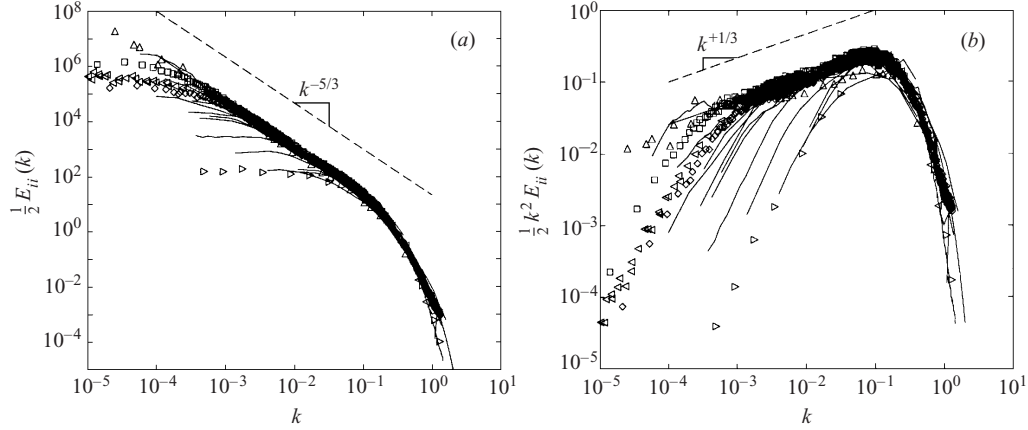


FIGURE 7. Kolmogorov's universal scaling for locally isotropic one-dimensional spectra ((a) energy spectra, (b) enstrophy spectra), from Saddoughi & Veeravalli (1994), for a variety of different turbulent flows; see Saddoughi & Veeravalli (1994) for descriptions of the various different experiments reported in this figure and discussion of the important effects of non-isotropy. A common explanation of turbulence is that turbulent energy is extracted from the mean-flow kinetic energy or potential energy at the low wavenumbers (large spatial scales), this energy cascades through the 'inertial range' by a vortex stretching phenomenon which transfers energy to higher wavenumbers, and the energy is ultimately dissipated by viscosity at the high wavenumbers (small spatial scales). The higher the Reynolds number, the longer this inertial range. As the energy cascade is largely unidirectional, the ultimate rate of turbulence dissipation at the small spatial scales is effectively set by the behaviour of the turbulence at the large spatial scales. As indicated in this figure, consideration of the energy in the cost functional focuses control effort primarily on the low wavenumbers of the turbulence spectrum, where the 'driving mechanisms' for turbulence lie, whereas consideration of the enstrophy in the cost functional focuses control effort on the high wave numbers of the turbulence spectrum, where the turbulence is dissipated.

smaller actuators than formulations derived from TKE-based cost functionals, which focus on the largest coherent motions of the turbulence. Such actuators might be much more challenging to build. These arguments favour TKE-based strategies over enstrophy-based strategies despite the mathematical preference (based on the Poincaré and Sobolev inequalities) to the contrary.

#### Case (d): regulation of large-scale and intermediate-scale structures

Due to considerations of both the physics of the phenomena at hand and its realization in hardware, we have argued that it might be better to control the large scales of turbulence rather than the small scales. We now show how this line of reasoning may be pursued even further. The idea is to select for the cost functional definition *lower* norms (e.g.  $H^{-1}$ ,  $H^{-2}$ , etc.) on the flow term and *higher* norms (e.g.  $H^1$ ,  $H^2$ , etc.) on the control term. This is now illustrated with a single example:

$$\mathcal{J}_{\text{LARGE(reg)}}(\phi) = -\frac{d_4}{2} \int_0^T \int_{\Omega} \mathbf{u}(\phi) \cdot \Delta^{-1} \mathbf{u}(\phi) \, dx \, dt - \frac{\ell^2}{2} \int_0^T \int_{\Gamma_{\pm}^{\pm}} \phi \Delta \phi \, dx \, dt.$$

Note that the term  $\xi \triangleq \Delta^{-1} \mathbf{u}$  is easily found by solving a Poisson equation  $\mathbf{u} = \Delta \xi$  with appropriate boundary conditions.

Effectively, such a cost functional targets a 'smoothed' version of the velocity field  $\mathbf{u}$ , weighting most heavily the low spatial wavenumbers of the velocity field, while

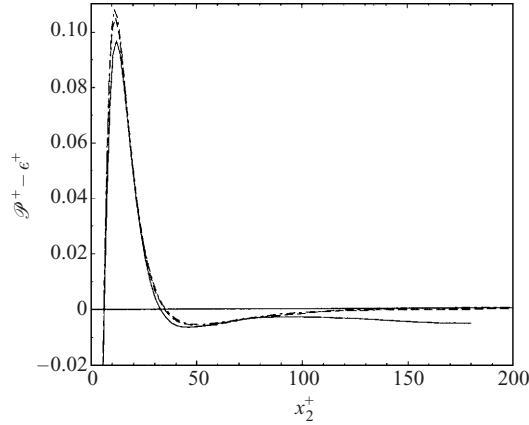


FIGURE 8. Excess energy production,  $\mathcal{P} - \epsilon$ , in wall units, as a function of distance from the wall. Data compiled by Jimenez (1999), for uncontrolled turbulent channel flows at: —,  $Re_\tau = 180$ ; ----,  $Re_\tau = 395$ ; -·-,  $Re_\tau = 590$ ; see Jimenez (1999) for descriptions of the various different computations reported in this figure.

it penalizes the component of the control  $\phi$  which is not smooth, weighting most heavily the high spatial wavenumbers of the control. Control formulations based on cost functionals with even greater emphasis on the large-scale structures follow in a natural manner from this example by taking higher powers of  $(-\Delta)$ , and are left as an exercise to the reader. Note that this smoothing can also be extended to the temporal fluctuations by replacing the spatial operators  $(-\Delta)$  above with the operator  $(\partial/\partial t - \nu\Delta)$ ; this particular type of smoothing is motivated by the linear terms of the Navier–Stokes equation itself.

In a turbulent channel flow at statistical equilibrium, the equation expressing the production, redistribution, and dissipation of the turbulent kinetic energy, referred to as the turbulent energy budget (Tennekes & Lumley 1972), is

$$\frac{\partial}{\partial x_2} \underbrace{\left( \overline{v_2 p} + \frac{1}{2} \overline{v_i v_i v_2} - 2\nu \overline{v_i s_{i2}} \right)}_{\text{energy flux}} = \underbrace{-\overline{v_1 v_2} \frac{\partial \overline{u_1}}{\partial x_2}}_{\mathcal{P}} - \underbrace{2\nu \overline{s_{ij} s_{ij}}}_{\epsilon}$$

where  $s_{ij} \triangleq 1/2 (\partial v_i / \partial x_j + \partial v_j / \partial x_i)$  and  $v_i = u_i - \overline{u_i}$  denotes the fluctuating components of the velocity field. The energy flux terms serve to redistribute the turbulent energy from one point in the flow to another. The ‘production’ term  $\mathcal{P}$  normally extracts energy from the mean flow  $\overline{u_1}$  to ‘feed’ the turbulent energy cascade, whereas the viscous dissipation term  $\epsilon$  dissipates energy from the turbulent cascade to the local environment by molecular (viscous) heating. The variation of the excess of production minus dissipation as a function of distance from the wall is shown in figure 8.

A substantial counter-argument to that for control of primarily the large scales of the turbulence may now be made for the case of wall-bounded turbulence treated in the present paper. The production of turbulence at the length scales of the coherent structures in the ‘inner layer’ near the wall ( $x_2^+ \lesssim 60$ ) is thought by some to have important communication with the larger scales in the outer layer via an ‘inverse

cascade' of energy<sup>†</sup> (Jimenez 1999). As illustrated in figures 5(a) and 6(a), there is a clear 'coherent-structure scale' to the turbulence near the wall of about 50 wall units which (at least, at the higher Reynolds numbers of engineering significance) certainly must be considered as intermediate between the large outer scales and the small dissipation scales. As shown in the  $\mathcal{P} - \epsilon$  spike of figure 8 near  $x_2^+ \approx 12$ , it is this near-wall turbulence which dominates the turbulence production in the turbulent energy budget. This observation extends at least over the limited range of Reynolds numbers reported in the DNS results compiled in this figure. One may therefore hypothesize that the coherent structures themselves are a primary 'cause' of the entire spectrum of wall-bounded turbulence, and target the flow perturbations at the specific length scale of these flow structures by employing a 'bandpass filter' of sorts. A very simple and algebraically convenient form of such a bandpass filter may be defined such that

$$\mathcal{J}_{\text{INT}(\text{reg})}(\phi) = -\frac{d_5}{2} \int_0^T \int_{\Omega} \mathbf{u}(\phi) \cdot \Delta_B^{-1} \mathbf{u}(\phi) \, d\mathbf{x} \, dt - \frac{\ell^2}{2} \int_0^T \int_{\Gamma_2^+} \phi \Delta_B \phi \, d\mathbf{x} \, dt.$$

where

$$\Delta_B = \Delta_S + \Delta_S^{-1} \quad \text{with} \quad \Delta_S = L_c^2 \Delta \quad \text{and} \quad L_c^+ = 50.$$

To motivate the use of such a filter, note that, in a spectral direction, the influence of this filter on the Fourier transform of the velocity field is  $\sim k^2/(k^4 + k_c^4)$ , a function which is small for both large  $k$  and small  $k$  and peaks at the wavenumber of interest,  $k_c$ , of the near-wall coherent structures. As for the large-scale filter, powers of  $(-\Delta_B)$  may be used for faster roll-off away from the spatial wavenumber of interest.

For high Reynolds number flows, a counter-argument may be made to that for the control of the coherent-structure scale of the flow. The phenomenon central to this argument, known as 'shear sheltering', is perhaps best known for the problem of plasma confinement in a tokamak fusion reactor, for which reversed magnetic shear greatly reduces the energy flux in the plasma (Kepner, Parker & Decyk 1997). Though the problems of fluid turbulence and plasma turbulence are fundamentally different, Hunt & Durbin (1999) propose that the region of high shear might similarly insulate the near-wall region from the outer region of a high-Reynolds-number turbulent boundary layer. Jacobs & Durbin (1998) provide some evidence for this by examination of linear fluctuations to a mean boundary-layer profile, observing that the shapes of the eigenmodes corresponding to the discrete and continuous spectra of the Orr–Sommerfeld equation are supported only in the near-wall and outer regions respectively. If, as this argument implies, the high shear of a high-Reynolds-number turbulent flow successfully blocks the major fraction of the turbulent cascade of energy across the high shear region, it may indeed be better to target the large spatial scales (to affect the outer-layer structures) rather than the coherent-structure scales (to affect the near-wall structures).

As there are many fewer degrees of freedom in the large scales or intermediate scales of turbulence than there are in its complete spectrum, formulations which target

<sup>†</sup> Note that a convincing argument can be made about the importance of the cascade of energy from small scales to large scales in turbulent flows in general. Gibson (1996) observes that in most flows of engineering interest (homogeneous isotropic turbulence being the notable exception), vorticity is introduced into irrotational regions in the flow at the small viscous scales through thin shear layers. If 'turbulence' is defined as the region in the flow where inertial forces ( $\mathbf{v} \times \boldsymbol{\omega}$ ) dominate viscous forces, then the irrotational regions of the flow ( $\boldsymbol{\omega} = \mathbf{0}$ ) must certainly be described as 'non-turbulent', and the importance of the so-called 'inverse cascade' (from small scales to large scales) in the overall energy budget is readily apparent.

either large-scale or coherent-structure-scale fluctuations in the flow might be expected to be better behaved numerically than TKE-based formulations, as the optimizations they entail are, effectively, lower dimensional and thus easier to perform. Though it is still the topic of some debate precisely which scales should be targeted by the control algorithm, the present method is sufficiently general to target whichever scales are of interest. Indeed, an interesting future use of the approach developed in this paper, once computers become fast enough to consider higher Reynolds numbers in this framework, is to shed light on this argument by comparing the effectiveness of controls targeting the large scales of turbulent boundary layers with that of controls targeting the coherent-structure scales of turbulent boundary layers.

*Case (e): terminal control of turbulent kinetic energy*

As described at the end of §2.1, it is appropriate to consider a cost functional which targets the *terminal value* (i.e. the value at the end of each optimization horizon) of the quantity of interest. We will illustrate with the example of the terminal control of turbulent kinetic energy. With the terminal control approach, the cost functional is not penalized for excursions of the turbulent kinetic energy during the middle of each optimization horizon, so long as these excursions lead to reduced values of the turbulent kinetic energy at the end of each optimization horizon. As referred to in the chess analogy, this is akin to ‘sacrificing’ a piece in order to obtain long-term gain. A relevant cost functional for this approach is

$$\mathcal{J}_{\text{TKE(ter)}}(\phi) = \frac{d_6}{2} \int_{\Omega} |\mathbf{u}(\phi; T)|^2 \, d\mathbf{x} + \frac{\ell^2}{2} \int_0^T \int_{\Gamma_{\pm}^{\pm}} \phi^2 \, d\mathbf{x} \, dt.$$

6.2. *Gradient of cost functional: general discussion*

As suggested by Abergel & Temam (1990), a rigorous procedure may be developed to determine the sensitivity of a cost functional  $\mathcal{J}$  to small modifications of the control  $\phi$  for Navier–Stokes control problems of this sort. To do this, consider the linearized perturbation  $\mathcal{J}'$  to the cost functional  $\mathcal{J}$  resulting from an arbitrary perturbation  $\phi'$  to the control  $\phi$ . The quantity  $\mathcal{J}'$  may be defined by a limiting process as the Fréchet differential (Vainberg 1964) of the cost functional  $\mathcal{J}$  with respect to  $\phi$  such that

$$\mathcal{J}'(\phi; \phi') \triangleq \lim_{\epsilon \rightarrow 0} \frac{\mathcal{J}(\phi + \epsilon\phi') - \mathcal{J}(\phi)}{\epsilon} \triangleq \int_0^T \int_{\Gamma_{\pm}^{\pm}} \frac{\mathcal{D}\mathcal{J}(\phi)}{\mathcal{D}\phi} \phi' \, d\mathbf{x} \, dt. \quad (6.1)$$

For the cases of interest here, the linearized cost functional perturbations  $\mathcal{J}'$  resulting from a control perturbation  $\phi'$  may be written as<sup>†</sup>

$$\mathcal{J}'_{\text{DRAG}}(\phi; \phi') = -d_1 \int_0^T \int_{\Gamma_{\pm}^{\pm}} v \frac{\partial u_1'}{\partial n} \, d\mathbf{x} \, dt + \ell^2 \int_0^T \int_{\Gamma_{\pm}^{\pm}} \phi\phi' \, d\mathbf{x} \, dt,$$

$$\mathcal{J}'_{\text{TKE(reg)}}(\phi; \phi') = d_2 \int_0^T \int_{\Omega} \mathbf{u} \cdot \mathbf{u}' \, d\mathbf{x} \, dt + \ell^2 \int_0^T \int_{\Gamma_{\pm}^{\pm}} \phi\phi' \, d\mathbf{x} \, dt,$$

$$\mathcal{J}'_{\text{ENS(reg)}}(\phi; \phi') = -d_3 \int_0^T \int_{\Omega} \Delta \mathbf{u} \cdot \mathbf{u}' \, d\mathbf{x} \, dt + \ell^2 \int_0^T \int_{\Gamma_{\pm}^{\pm}} \phi\phi' \, d\mathbf{x} \, dt,$$

<sup>†</sup> Note that, for the remainder of this discussion, the functional dependence of  $\mathbf{u}$  on  $\phi$  is suppressed for notational clarity.

$$\begin{aligned}\mathcal{J}'_{\text{LARGE}(\text{reg})}(\phi; \phi') &= -d_4 \int_0^T \int_{\Omega} \Delta^{-1} \mathbf{u} \cdot \mathbf{u}' \, d\mathbf{x} \, dt - \ell^2 \int_0^T \int_{\Gamma_{\frac{\pm}{2}}} \Delta \phi \phi' \, d\mathbf{x} \, dt, \\ \mathcal{J}'_{\text{INT}(\text{reg})}(\phi; \phi') &= -d_5 \int_0^T \int_{\Omega} \Delta_B^{-1} \mathbf{u} \cdot \mathbf{u}' \, d\mathbf{x} \, dt - \ell^2 \int_0^T \int_{\Gamma_{\frac{\pm}{2}}} \Delta_B \phi \phi' \, d\mathbf{x} \, dt, \\ \mathcal{J}'_{\text{TKE}(\text{ter})}(\phi; \phi') &= d_6 \int_{\Omega} \mathbf{u}(T) \cdot \mathbf{u}'(T) \, d\mathbf{x} + \ell^2 \int_0^T \int_{\Gamma_{\frac{\pm}{2}}} \phi \phi' \, d\mathbf{x} \, dt,\end{aligned}$$

where  $\mathbf{u}'$  is the Fréchet differential of  $\mathbf{u}$ , as defined in the following subsection, and where we have made use of the identity  $\Delta \mathbf{u} = -\nabla \times (\nabla \times \mathbf{u})$  (for  $\nabla \cdot \mathbf{u} = 0$ ) and the fact that the curl operator ( $\nabla \times$ ), the Laplacian ( $\Delta$ ), and the bandpass filter ( $\Delta_B$ ) are self-adjoint.

For each of the cost functionals under consideration, the linearized cost functional perturbation  $\mathcal{J}'$  will be expressed as a simple linear convolution of some function of an appropriately defined adjoint field  $\mathbf{q}^*$  with the control perturbation  $\phi'$ , in a form identical to the right-hand side of (6.1). As the resulting expression holds for arbitrary  $\phi'$ , the gradient  $\mathcal{D}\mathcal{J}(\phi)/\mathcal{D}\phi$  may be identified immediately with this function of the solution to the adjoint problem. Mathematically, we say that  $\mathcal{D}\mathcal{J}(\phi)/\mathcal{D}\phi$  is identified in a ‘weak’ sense by such a procedure. Note that, in a finite-dimensional setting (i.e. when the problem is discretized in space and time), the gradient takes the form of a Jacobian of the scalar quantity  $\mathcal{J}(\phi)$  with respect to the individual components of the (very high-dimensional) discretized vector  $\phi$ .

With the gradient information so determined, any control  $\phi$  on  $(0, T)$  may be updated in the direction that, at least locally (i.e. for infinitesimal control updates), most effectively reduces the cost functional of interest. The finite distance the control is updated in this direction is determined with a line minimization algorithm. (This makes the iteration procedure very efficient and stable, even when considering inherently nonlinear phenomena, by guaranteeing that the cost functional of interest at least will not increase from one iteration to the next.) The flow resulting from this updated control is then computed, the sensitivity of this new flow to further control modification is determined via the computation of a new adjoint field, and the process repeated. Upon convergence of this iteration, which locally optimizes the control over the interval  $(0, T)$ , the flow is advanced with the optimized controls over the horizon  $(0, T_a)$ , where  $T_a \leq T$ , and an iteration for the optimal control over a new time horizon begins anew on the interval  $(T_a, T_a + T)$ , as discussed in the introduction to the receding horizon framework given in §2.1.

Note that, as opposed to the controls computed near the beginning of each optimization horizon, the controls computed near the end of each optimization horizon are determined without regard to the (inevitable) further development of the flow. The controls near the end of each optimization horizon (on  $(T_a, T)$ ) may thus not be as effective as the controls near the beginning of each optimization horizon (on  $(0, T_a)$ ) for long-time regulation of the system (i.e. looking beyond the interval  $(0, T)$  represented in the cost function). Thus, in the standard ‘receding horizon model predictive control’ framework (see, e.g. Soeterboek 1992 and Bitmead, Gevers & Wertz 1990 for further details), the controls on  $(T_a, T)$  are often discarded and recalculated in the following optimization horizon. This is analogous to the repeated re-evaluation of the game plan necessary after each move played during a game of chess: one optimizes the game plan over several moves, plays just one move, then repeats the optimization process. To expediate the computations, all computations reported here

in fact take  $T_a = T$  except for one curve reported in figure 15, where the issue of taking  $T_a < T$  is revisited.

### 6.2.1. Linearized perturbation field

Now consider the linearized perturbation  $\mathbf{q}'$  to the flow  $\mathbf{q}$  resulting from a perturbation  $\phi'$  to the control  $\phi$ . Again, the quantity  $\mathbf{q}'$  may be defined by the limiting process of a Fréchet differential such that

$$\mathbf{q}' \triangleq \lim_{\epsilon \rightarrow 0} \frac{\mathbf{q}(\phi + \epsilon\phi') - \mathbf{q}(\phi)}{\epsilon}. \quad (6.2)$$

For the purpose of gaining physical intuition, it is useful to note that the quantity  $\mathbf{q}'$ , described above as a differential quantity, may instead be defined as the small perturbation to the state  $\mathbf{q}$  arising from a small control perturbation  $\phi'$  to the control  $\phi$ . In such derivations, the notation  $\delta\phi$  and  $\delta\mathbf{q}$ , denoting small perturbations to  $\phi$  and  $\mathbf{q}$ , is used instead of the differential quantities  $\phi'$  and  $\mathbf{q}'$ . The two derivations are roughly equivalent, though the present derivation does not assume that primed quantities are small, rather, only that they are defined by a limiting process such as (6.2).

The equation governing the dependence of the linearized flow perturbation  $\mathbf{q}'$  on the control perturbation  $\phi'$  may be found by taking the Fréchet differential of the state equation 3.1. The result is

$$\mathcal{N}'(\mathbf{q})\mathbf{q}' = 0 \quad \text{in } \Omega, \quad (6.3a)$$

$$\mathbf{u}' = -\phi'\mathbf{n} \quad \text{on } \Gamma_2^\pm, \quad (6.3b)$$

$$\mathbf{u}' = 0 \quad \text{at } t = 0, \quad (6.3c)$$

where the linearized Navier–Stokes operation  $\mathcal{N}'(\mathbf{q})\mathbf{q}'$  is given by

$$\mathcal{N}'(\mathbf{q})\mathbf{q}' = \left( \begin{array}{c} \frac{\partial u'_j}{\partial x_j} \\ \frac{\partial u'_i}{\partial t} + \frac{\partial}{\partial x_j}(u_j u'_i + u'_j u_i) - \nu \frac{\partial^2 u'_i}{\partial x_j^2} + \frac{\partial p'}{\partial x_i} \end{array} \right). \quad (6.4)$$

The operation  $\mathcal{N}'(\mathbf{q})\mathbf{q}'$  is a linear operation on the perturbation field  $\mathbf{q}'$ , though the operator  $\mathcal{N}'(\mathbf{q})$  is itself a function of the solution  $\mathbf{q}$  of the Navier–Stokes problem—note the presence of the velocity field  $\mathbf{u}$  in (6.4). Equation (6.3) thus reflects the linear dependence of the perturbation field  $\mathbf{q}'$  in the interior of the domain on the control perturbation  $\phi'$  at the boundary. However, the implicit linear relationship  $\mathbf{q}' = \mathbf{q}'(\phi')$  given by this equation is not yet tractable for expressing  $\mathcal{J}'$  in a form similar to the right hand side of (6.1), from which  $\mathcal{D}\mathcal{J}(\phi)/\mathcal{D}\phi$  may be deduced. For the purpose of determining a more useful relationship with which we may determine  $\mathcal{D}\mathcal{J}(\phi)/\mathcal{D}\phi$ , we now appeal to an adjoint identity.

### 6.2.2. Derivation of adjoint identity

This subsection derives the adjoint of the linear partial differential operator  $\mathcal{N}'(\mathbf{q})$ . For readers not familiar with this approach, a review of the derivation of an adjoint operator for a very simple case in the present notation is given in Appendix A. The adjoint derivation presented below extends in a straightforward manner to more complex equations, such as the compressible Euler equation, as shown in Appendix B (again, using the same notation). Such generality highlights the versatility of the present approach.

Define an inner product over the domain in space–time under consideration such that

$$\langle \mathbf{q}', \mathbf{q}^* \rangle = \int_0^T \int_{\Omega} \mathbf{q}' \cdot \mathbf{q}^* \, d\mathbf{x} \, dt,$$

and consider the identity

$$\boxed{\langle \mathcal{N}'(\mathbf{q})\mathbf{q}', \mathbf{q}^* \rangle = \langle \mathbf{q}', \mathcal{N}'(\mathbf{q})^* \mathbf{q}^* \rangle + b.} \quad (6.5)$$

Integration by parts may be used to move all differential operations from  $\mathbf{q}'$  on the left-hand side of (6.5) to  $\mathbf{q}^*$  on the right-hand side, resulting in the definition of the adjoint operator

$$\mathcal{N}'(\mathbf{q})^* \mathbf{q}^* = \left( \begin{array}{c} -\frac{\partial u_j^*}{\partial x_j} \\ -\frac{\partial u_i^*}{\partial t} - u_j \left( \frac{\partial u_i^*}{\partial x_j} + \frac{\partial u_j^*}{\partial x_i} \right) - v \frac{\partial^2 u_i^*}{\partial x_j^2} - \frac{\partial p^*}{\partial x_i} \end{array} \right), \quad (6.6)$$

where, again, the operation  $\mathcal{N}'(\mathbf{q})^* \mathbf{q}^*$  is a linear operation on the adjoint field  $\mathbf{q}^*$ , and the operator  $\mathcal{N}'(\mathbf{q})^*$  is itself a function of the solution  $\mathbf{q}$  of the Navier–Stokes problem. From the integrations by parts, we also get several boundary terms:

$$b = \int_{\Omega} (u_j^* u_j') \Big|_{t=0}^{t=T} \, d\mathbf{x} + \int_0^T \int_{\Gamma_2^{\pm}} n_j \left[ p^* u_j' + u_i^* (u_j u_i' + u_j' u_i) - v \left( u_i^* \frac{\partial u_i'}{\partial x_j} - u_i' \frac{\partial u_i^*}{\partial x_j} \right) + u_j^* p' \right] \, d\mathbf{x} \, dt,$$

where  $\mathbf{n}$  denotes a unit outward normal to the surface. The quantity  $b$  is closely related to the bilinear concomitant discussed by Morse & Feshbach (1953), and the outline of the present derivation is related to the approach taken therein.

The identity (6.5) is the key to expressing  $\mathcal{J}'$  in the desired form. An adjoint field  $\mathbf{q}^*$  is first defined using the operator  $\mathcal{N}'(\mathbf{q})^*$  together with appropriate forcing in an interior equation with appropriate boundary conditions and initial conditions. There is here some flexibility which we exploit to obtain a simple expression for  $\mathcal{J}'$ . Indeed, combining this definition of  $\mathbf{q}^*$  with the definitions of  $\mathbf{q}$  in (3.1) and  $\mathbf{q}'$  in (6.3), the identity (6.5) reveals the desired expression, as will now be shown for the cases of interest in this paper.

### 6.2.3. Definition of adjoint field and identification of gradient

#### Case (a): minimization of drag

Consider an adjoint state defined (as yet, arbitrarily) by

$$\mathcal{N}'(\mathbf{q})^* \mathbf{q}^* = 0 \quad \text{in } \Omega, \quad (6.7a)$$

$$\mathbf{u}^* = -d_1 \mathbf{r} \quad \text{on } \Gamma_2^{\pm}, \quad (6.7b)$$

$$\mathbf{u}^* = 0 \quad \text{at } t = T, \quad (6.7c)$$

where the adjoint operation  $\mathcal{N}'(\mathbf{q})^* \mathbf{q}^*$  is given in (6.6) and  $\mathbf{r}$  is a unit vector in the  $x_1$ -direction. Note that the adjoint problem (6.7), though linear, has complexity similar to that of the Navier–Stokes problem (3.1), and may be solved with similar numerical methods. Note also that the ‘initial’ conditions in (6.7) are defined at  $t = T$ , and are thus best referred to as ‘terminal’ conditions. With this definition, the adjoint field

must be marched *backward* in time over the optimization horizon—due to the sign of the time derivative and viscous terms in the adjoint operator  $\mathcal{N}'(\mathbf{q})^*$  in (6.6), this is the natural direction for this time march. However, as the operator  $\mathcal{N}'(\mathbf{q})^*$  is a function of  $\mathbf{q}$ , computation of the adjoint field  $\mathbf{q}^*$  requires storage of the flow field  $\mathbf{q}$  on  $t \in [0, T]$ , which itself must be computed with a *forward* march. This storage issue presents one of the numerical complications which preclude solution of the present optimization problem for large optimization intervals  $T$ . However, the problem is not insurmountable for intermediate values of  $T^+ \lesssim O(100)$ .

The identity (6.5) is now simplified using the equations defining the state field (3.1), the perturbation field (6.3), and the adjoint field (6.7). Due to the judicious choice of the right-hand-side forcing to the adjoint problem in (6.7b), the identity (6.5) reduces (after some manipulation) to

$$-d_1 \int_0^T \int_{\Gamma_2^\pm} v \frac{\partial u'_1}{\partial n} \, d\mathbf{x} \, dt = \int_0^T \int_{\Gamma_2^\pm} p^* \phi' \, d\mathbf{x} \, dt.$$

Using this equation, the cost functional perturbation  $\mathcal{J}'_{\text{DRAG}}$  may be rewritten as

$$\mathcal{J}'_{\text{DRAG}}(\phi; \phi') = \int_0^T \int_{\Gamma_2^\pm} \frac{\mathcal{D} \mathcal{J}_{\text{DRAG}}(\phi)}{\mathcal{D} \phi} \phi' \, d\mathbf{x} \, dt = \int_0^T \int_{\Gamma_2^\pm} (p^* + \ell^2 \phi) \phi' \, d\mathbf{x} \, dt.$$

As  $\phi'$  is arbitrary, this implies that

$$g_{\text{DRAG}} \triangleq \frac{\mathcal{D} \mathcal{J}_{\text{DRAG}}(\phi)}{\mathcal{D} \phi} = p^* + \ell^2 \phi.$$

The desired gradient  $\mathcal{D} \mathcal{J}_{\text{DRAG}}(\phi)/\mathcal{D} \phi$  is thus found to be a simple function of the solution of the adjoint problem proposed in (6.7).

*Case (b): regulation of turbulent kinetic energy*

Consider an adjoint state defined by

$$\mathcal{N}'(\mathbf{q})^* \mathbf{q}^* = d_4 \begin{pmatrix} 0 \\ \mathbf{u} \end{pmatrix} \quad \text{in } \Omega, \quad (6.8a)$$

$$\mathbf{u}^* = 0 \quad \text{on } \Gamma_2^\pm, \quad (6.8b)$$

$$\mathbf{u}^* = 0 \quad \text{at } t = T. \quad (6.8c)$$

The identity (6.5) is now simplified using the equations defining the state field (3.1), the perturbation field (6.3), and the adjoint field (6.8). Due to the judicious choice of the right-hand-side forcing to the adjoint problem in (6.8a), the identity (6.5) reduces to

$$d_4 \int_0^T \int_{\Omega} \mathbf{u} \cdot \mathbf{u}' \, d\mathbf{x} \, dt = \int_0^T \int_{\Gamma_2^\pm} p^* \phi' \, d\mathbf{x} \, dt.$$

Using this equation, the cost functional perturbation  $\mathcal{J}'_{\text{TKE}(\text{reg})}$  may be rewritten in the desired form, as in case (a), and thus, as  $\phi'$  is arbitrary, we find that

$$g_{\text{TKE}(\text{reg})} \triangleq \frac{\mathcal{D} \mathcal{J}_{\text{TKE}(\text{reg})}}{\mathcal{D} \phi} = p^* + \ell^2 \phi.$$

The desired gradient  $\mathcal{D} \mathcal{J}_{\text{TKE}(\text{reg})}(\phi)/\mathcal{D} \phi$  is thus found to be a simple function of the solution of the adjoint problem proposed in (6.8).

Case (c): regulation of enstrophy

Consider an adjoint state defined by

$$\mathcal{N}'(\mathbf{q})^* \mathbf{q}^* = d_3 \begin{pmatrix} 0 \\ -\Delta \mathbf{u} \end{pmatrix} \quad \text{in } \Omega, \quad (6.9a)$$

$$\mathbf{u}^* = 0 \quad \text{on } \Gamma_2^\pm, \quad (6.9b)$$

$$\mathbf{u}^* = 0 \quad \text{at } t = T. \quad (6.9c)$$

The identity (6.5) is now simplified using the equations defining the state field (3.1), the perturbation field (6.3), and the adjoint field (6.9). Due to the judicious choice of the right-hand-side forcing to the adjoint problem in (6.9a), the identity (6.5) reduces to

$$-d_3 \int_0^T \int_\Omega \Delta \mathbf{u} \cdot \mathbf{u}' \, d\mathbf{x} \, dt = \int_0^T \int_{\Gamma_2^\pm} p^* \phi' \, d\mathbf{x} \, dt.$$

Using this equation, the cost functional perturbation  $\mathcal{J}'_{\text{ENS(reg)}}$  may be rewritten in the desired form, as in case (a), and thus, as  $\phi'$  is arbitrary, we find that

$$g_{\text{ENS(reg)}} \triangleq \frac{\mathcal{D} \mathcal{J}_{\text{ENS(reg)}}}{\mathcal{D} \phi} = p^* + \ell^2 \phi.$$

The desired gradient  $\mathcal{D} \mathcal{J}_{\text{ENS(reg)}}(\phi)/\mathcal{D} \phi$  is thus found to be a simple function of the solution of the adjoint problem proposed in (6.9).

Case (d): regulation of large-scale and intermediate-scale structures

Consider an adjoint state defined by

$$\mathcal{N}'(\mathbf{q})^* \mathbf{q}^* = d_4 \begin{pmatrix} 0 \\ -\Delta^{-1} \mathbf{u} \end{pmatrix} \quad \text{in } \Omega, \quad (6.10a)$$

$$\mathbf{u}^* = 0 \quad \text{on } \Gamma_2^\pm, \quad (6.10b)$$

$$\mathbf{u}^* = 0 \quad \text{at } t = T. \quad (6.10c)$$

The identity (6.5) is now simplified using the equations defining the state field (3.1), the perturbation field (6.3), and the adjoint field (6.10). Due to the judicious choice of the right-hand-side forcing to the adjoint problem in (6.10a), the identity (6.5) reduces to

$$-d_4 \int_0^T \int_\Omega \Delta^{-1} \mathbf{u} \cdot \mathbf{u}' \, d\mathbf{x} \, dt = \int_0^T \int_{\Gamma_2^\pm} p^* \phi' \, d\mathbf{x} \, dt.$$

Using this equation, the cost functional perturbation  $\mathcal{J}'_{\text{LARGE(reg)}}$  may be rewritten in the desired form, as in case (a), and thus, as  $\phi'$  is arbitrary, we find that

$$g_{\text{LARGE(reg)}} \triangleq \frac{\mathcal{D} \mathcal{J}_{\text{LARGE(reg)}}}{\mathcal{D} \phi} = p^* - \ell^2 \Delta \phi.$$

The desired gradient  $\mathcal{D} \mathcal{J}_{\text{LARGE(reg)}}(\phi)/\mathcal{D} \phi$  is thus found to be a simple function of the solution of the adjoint problem proposed in (6.10).

The formulation following from  $\mathcal{J}_{\text{INT(reg)}}$  is identical to that for  $\mathcal{J}_{\text{LARGE(reg)}}$  with  $\Delta$  replaced by  $\Delta_B$ .

Case (e): terminal control of turbulent kinetic energy

Consider an adjoint state defined by

$$\mathcal{N}'(\mathbf{q})^* \mathbf{q}^* = 0 \quad \text{in } \Omega, \quad (6.11a)$$

$$\mathbf{u}^* = 0 \quad \text{on } \Gamma_2^\pm, \quad (6.11b)$$

$$\mathbf{u}^* = d_6 \mathbf{u}(T) \quad \text{at } t = T. \quad (6.11c)$$

The identity (6.5) is now simplified using the equations defining the state field (3.1), the perturbation field (6.3), and the adjoint field (6.11). Due to the judicious choice of the right-hand-side forcing to the adjoint problem in (6.11), the identity (6.5) reduces to

$$d_6 \int_{\Omega} \mathbf{u}(T) \cdot \mathbf{u}'(T) d\mathbf{x} = \int_0^T \int_{\Gamma_2^\pm} p^* \phi' d\mathbf{x} dt.$$

Using this equation, the cost functional perturbation  $\mathcal{J}'_{\text{TKE(ter)}}$  may be rewritten in the desired form, as in case (a), and thus, as  $\phi'$  is arbitrary, we find that

$$g_{\text{TKE(ter)}} \triangleq \frac{\mathcal{D} \mathcal{J}_{\text{TKE(ter)}}}{\mathcal{D} \phi} = p^* + \ell^2 \phi.$$

The desired gradient  $\mathcal{D} \mathcal{J}_{\text{TKE(ter)}}(\phi) / \mathcal{D} \phi$  is thus found to be a simple function of the solution of the adjoint problem proposed in (6.11).

#### 6.2.4. The general framework

In the cases studied in the previous subsection, three possible locations of forcing for the adjoint problem were encountered: the interior equation, as in (6.8a), (6.9a) and (6.10a), the boundary conditions, as in (6.7b), and the terminal conditions, as in (6.11c). The domain of forcing appropriate for the adjoint problem is strictly a function of the domain in which cost functional to be minimized weights the flow quantities.

In this paper, we only consider control of the flow by modification of the boundary conditions (blowing/suction). In addition, however, the flow problem may be forced by interior forcing (such as the Lorentz force exerted by electromagnetic fields on a conducting fluid) or optimized with respect to its initial conditions (a situation that arises in forecasting problems). Thus, there is a duality between the three possible sources of forcing in the flow problem and the three possible sources of forcing in the adjoint problem. This general mathematical framework is laid out in detail in Bewley *et al.* (2000).

### 6.3. Gradient update to the control

#### 6.3.1. Simple gradient

With the gradient information determined in the previous subsection, a strategy for optimization of the controls using a simple gradient algorithm may be proposed such that

$$\phi^{k+1} = \phi^k - \alpha^k g^k$$

over the entire optimization horizon  $t \in (0, T)$ , where  $k$  indicates the iteration number and  $\alpha^k$  is a parameter of descent which governs how large an update is made. At each iteration,  $\alpha^k$  is computed to be that value which locally minimizes the cost functional  $\mathcal{J}(\phi)$  under consideration when the control  $\phi^k$  is updated in the direction  $-g^k$  of local maximum decrease of the cost functional  $\mathcal{J}(\phi^k)$ . This minimization is conducted with a numerically stable line search algorithm. The iteration is initialized with  $\phi^1 = 0$ . As  $k \rightarrow \infty$ , such an algorithm will usually converge to some local minimum of  $\mathcal{J}(\phi)$ . Note that, due to the nonlinearity of the system, convergence to the global minimum

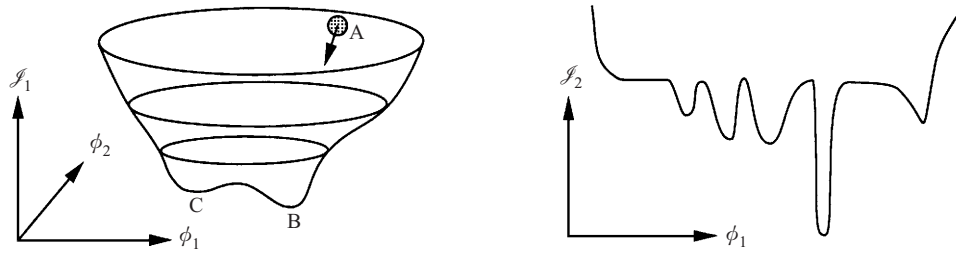


FIGURE 9. Possible shortcoming of gradient-based approaches: convergence to local minima.

will not in general be attained by such a scheme and that, as time proceeds,  $\mathcal{J}$  will not necessarily decrease.

To visualize the minimization problem in a low-dimensional setting, figure 9 illustrates the possible shape of a cost function  $\mathcal{J}_1(\phi_1, \phi_2)$  in the space spanned by the setting of two control variables  $\phi_1$  and  $\phi_2$  in a discrete low-dimensional optimization problem. As shown in the figure, there will be some minimum point away from which the value of the cost function will be higher, and thus the shape of the cost function in this space might look something like a deformed bowl. Starting from point A in figure 9, computation of the appropriately defined adjoint field provides information about the local shape of the bowl, as indicated by the shaded region: specifically, it identifies the direction of maximum decrease of the cost function, indicated by the arrow. By continually moving in the direction of steepest descent, the simple gradient algorithm eventually proceeds towards a minimum of the cost function. Note, however, that depending on where point A is relative to the minima, this algorithm may converge to the global minimum B or to some other local minimum such as C; this is a drawback of searching with a gradient routine. To alleviate this difficulty, the gradient search routine may be initialized from several different starting points  $\phi^{1,j}$  (chosen at random or from a regular array selected *a priori*), the optimization conducted from each starting point, and the performance of the different sets of optimized controls compared. Alternatively, a random disturbance can be added to the control update near the beginning of the optimization process (cooling this disturbance off near the end of the optimization) to ‘push’ the algorithm out of shallow local minima. Both approaches effectively blend the ‘global’ minimization capability of genetic algorithms with the fast convergence capability for very high-dimensional optimization problems of gradient-based algorithms, but neither approach was found to be necessary in the present work. Note that in pathological cases, such as the function  $\mathcal{J}_2(\phi_1)$  illustrated in figure 9, gradient algorithms break down altogether, and strategies based on function evaluations alone are preferred (see § 2.1).

### 6.3.2. Conjugate gradient

As shown in figure 10, the simple gradient approach described above is usually very inefficient. Even in quadratic minimization problems, for cases in which the function being minimized has a long, narrow ‘valley’, the simple gradient algorithm often gets stuck ‘bouncing’ from one side of the valley to the other without turning to proceed along the valley floor, as shown in figure 10(a)†. In such cases, the conjugate gradient

† Note that, in the present approach, a line minimization is performed at each iteration in the descent direction. The ‘bouncing’ behaviour shown in figure 10(a) may be alleviated somewhat by stopping short of a line minimization at each iteration, at the cost of slowing the convergence of the gradient algorithm significantly.

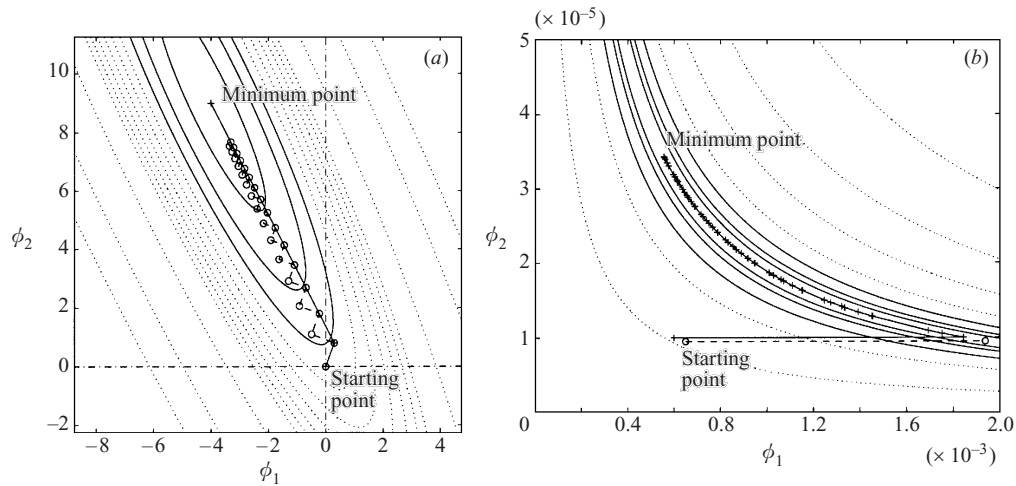


FIGURE 10. Convergence of the simple gradient algorithm ( $\circ$ ) and the Polak–Ribere variant of the conjugate gradient algorithm ( $+$ ), when applied to find minima of two test functions, (a) quadratic  $\mathcal{J}_3(\phi_1, \phi_2)$  and (b) non-quadratic  $\mathcal{J}_4(\phi_1, \phi_2)$ , of two scalar control variables  $\phi_1$  and  $\phi_2$  (horizontal and vertical axes). Contours illustrate the level surfaces of the test functions; contours corresponding to the smallest isovalues are solid, those corresponding to higher isovalues are dotted.

algorithm has proven to be much more efficient, at the very modest cost of a slight increase in computational storage. This method proceeds in a direction which is a linear combination of the direction of maximum decrease of the cost function and the direction used in the previous descent step. Thus, like a skier negotiating a similar type of terrain, this scheme retains a momentum term that helps turn the descent path to proceed down narrow valleys. Further, the conjugate gradient approach may be adapted to be quite effective even for non-quadratic minimization problems, as demonstrated in figure 10(b).

The model problem considered in figure 10(a) is the minimization of a simple function  $\mathcal{J}_3(\phi_1, \phi_2)$  which is quadratic in the control variables; this problem illustrates an extremely low-order model of the cost function for the present flow problem if the state equation is assumed to be linear (e.g. for small perturbations of  $\phi$  from the minimum point of  $\mathcal{J}(\phi)$ ). The model problem considered in figure 10(b) is a stiff chemical equilibrium problem to determine the equilibrium concentrations of the proton and carbonate species in a sodium bicarbonate solution; in this case, the function to be minimized,  $\mathcal{J}_4(\phi_1, \phi_2)$ , is a sixth-order polynomial in the control variables. In both cases, the conjugate gradient algorithm converges to within machine zero of the absolute minimum of  $J$ . Convergence is attained in 2 iterations in the quadratic case and 60 iterations in the non-quadratic case.

In contrast, the simple gradient algorithm does not converge effectively to the minimum in either of these two simple test problems, even though 30 iterations are used in the fairly well-conditioned quadratic problem of figure 10(a) and 1000 iterations are used in the poorly conditioned non-quadratic problem of figure 10(b). In fact, in the non-quadratic case, the simple gradient algorithm makes no visible progress towards the minimum after the first iteration for the particular initial conditions shown, resulting in an error of over a factor of 3 in both of the concentrations. Based on the results of these tests, the conjugate gradient algorithm was selected for all control optimizations reported in the remainder of this work.

The particular variant of the conjugate gradient algorithm which appears to be best suited for most non-quadratic optimization problems, including the difficult case

shown in figure 10(b), is referred to as the *Polak–Ribiere* method (Polak 1971; Scales 1985; Press *et al.* 1986; Luenberger 1989). It is given by

$$\phi^{k+1} = \phi^k + \alpha^k h^k,$$

where the update direction  $h^k$  is initialized such that  $h^1 = -g^1$  and defined thereafter by

$$h^k = -g^k + \beta^k h^{k-1},$$

where the gradient  $g^k$  is determined by an adjoint formulation for the cost functional of interest  $\mathcal{J}(\phi^k)$ , as discussed in §6.2, and the coefficient  $\beta^k$  in the momentum term is given by

$$\beta^k = \frac{(g^k - g^{k-1}) \cdot g^k}{g^{k-1} \cdot g^{k-1}}.$$

Again,  $\alpha^k$  is computed to be that value which minimizes the cost functional  $\mathcal{J}(\phi)$  under consideration when the control  $\phi^k$  is updated in the direction of descent  $h^k$ .

Applying this algorithm to minimize a quadratic function  $J(\phi)$ , the sequence of gradient vectors throughout the iteration are mutually orthogonal, so  $g^{k-1} \cdot g^k = 0$ . Neglecting numerical error, exact convergence is achieved in  $N$  iterations, where  $N$  is the dimension of the vector  $\phi$  being optimized, as shown in figure 10(a) for  $N = 2$ . For the minimization of non-quadratic functions, the term  $g^{k-1} \cdot g^k$  tends to reset the conjugate gradient iteration towards a simple gradient behaviour in non-quadratic regions, and thus, usually, speeds the convergence. However, such resetting behaviour is not fully reliable, and thus it is generally useful to ‘bleed off’ the excess momentum occasionally, taking  $\beta^k = 0$  every 10 or 20 iterations and thereby resetting to a simple gradient step before continuing.

The dimension of the control in the present problem is quite large ( $O(10^7)$  control variables per optimization horizon at  $Re_\tau = 180$  and  $T^+ = 40$ ), which precludes the use of second-order techniques which are based on the computation or approximation of the full Hessian matrix  $\partial^2 \mathcal{J} / \partial \phi_i \partial \phi_j$  or its inverse during the control optimization. The number of elements in such a matrix scales with the square of the number of control variables, and is unmanageable in the present case. However, reduced-storage variants of variable metric methods (Vanderplaats 1984), such as the Davidon–Fletcher–Powell (DFP) method, the Broydon–Fletcher–Goldfarb–Shanno (BFGS) method, and the sequential quadratic programming (SQP) method, approximate the inverse Hessian information by outer products of stored gradient vectors, and thus achieve nearly second-order convergence without storage of the full Hessian matrix. Such techniques should be explored further for very large-scale optimization problems such as the present in future work.

#### 6.4. Numerical method for control computation

The adjoint problem is discretized and coded with a numerical method almost identical to that used to solve the flow problem on the same spatial grid (see §4). The velocity field is stored every 5 time steps on the forward sweep, with linear interpolation of these stored fields used on the backward sweep to determine the operator  $\mathcal{N}'(\mathbf{q})^*$ . The Polak–Ribiere variant of the conjugate gradient algorithm is used for the control update, with  $\alpha$  computed at each iteration by Brent’s method, which is a stable and numerically efficient line-minimization algorithm taken from Press *et al.* (1986) which begins the optimization with a ‘safe’ golden section search and transfers to a ‘fast’ inverse parabolic interpolation when the solution is approached.

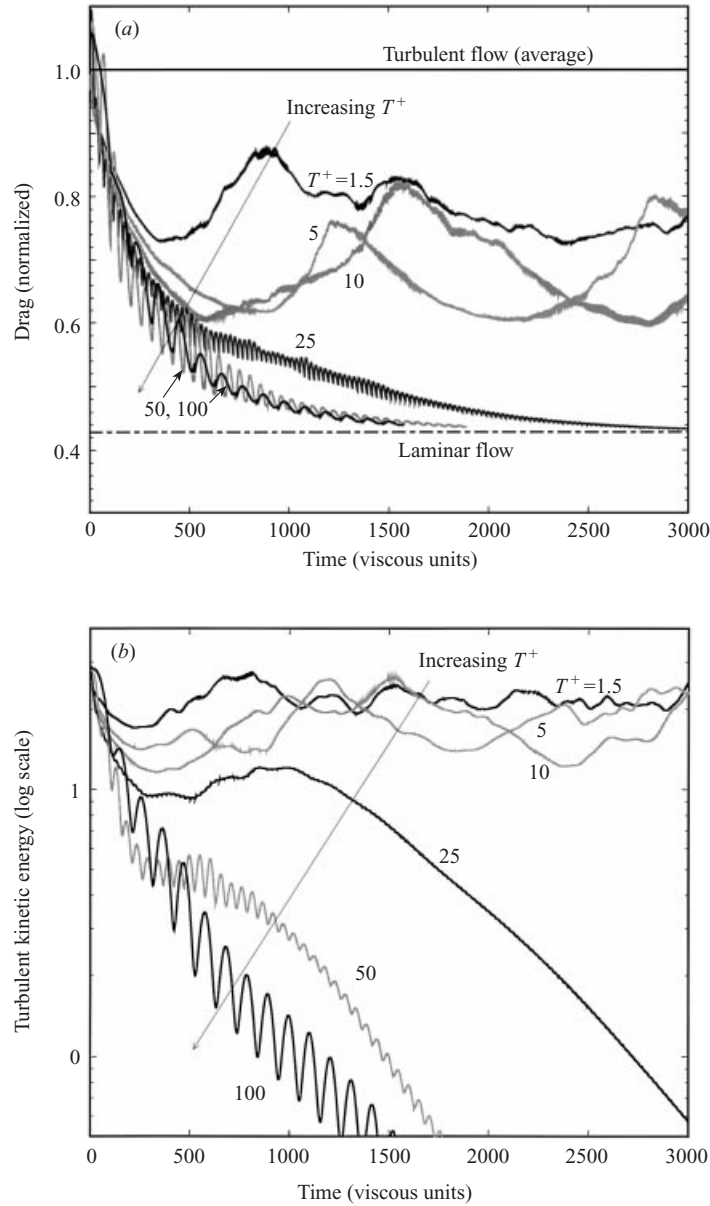


FIGURE 11. Performance of optimized controls for formulations based on  $\mathcal{J}_{\text{TKE}(\text{ter})}$  as a function of the optimization horizon  $T^+$  as computed in direct numerical simulations at  $Re_c = 100$ : (a) history of drag, (b) history of turbulent kinetic energy. For small optimization horizons ( $T^+ = O(1)$ ), approximately 20% drag reduction is obtained, a result which can be obtained with a variety of other approaches. For sufficiently large optimization horizons ( $T^+ \gtrsim 25$ ), the flow is returned to the region of stability of the laminar flow and the flow relaminarizes, resulting in a 57.2% drag reduction with no further control effort required.

## 7. Performance of controlled systems

In order to validate the utility of the DNS-based predictive control approach, a series of simulations was performed using the code outlined in §4 and benchmarked in §5. These simulations bring to light several of the control issues discussed previously.

The horizon  $T$  over which the flow is optimized is a critical parameter which must be chosen carefully. The larger the optimization horizon, the more the cost functional represents the problem of interest, but the more the optimization problem increases in difficulty. As mentioned previously, it appears as if optimization of the nonlinear Navier–Stokes control problem over an infinite time horizon, which would require the solution of a very difficult Hamilton–Jacobi–Bellman (HJB) problem in infinite dimension, is computationally intractable. As shown in figure 11, it is worthwhile to consider as long a  $T$  as computationally affordable in order to maximize long-term performance. Returning to the chess analogy (see §2.1), this makes perfect sense: one can never win a game of chess by looking forward in time just a single move. On the contrary, it is essential to estimate how the game will evolve. Note that relaminarization occurs in the present simulations for the  $\mathcal{J}_{\text{TKE(ter)}}$  formulations when  $T^+ \gtrsim 25$ . Note also that, for simplicity, we have taken  $T_a = T$  for all of the simulations reported here; variations of the ratio  $T_a/T$  are explored in figure 15.

The lobed behaviour of figure 11 is expected, and is a consequence of the fact that we are using here a formulation based on the terminal control of TKE in the receding-horizon framework. As discussed at the end of §2.1, such a strategy allows excursions of the TKE over the short term to go unpenalized by the control algorithm so long as they lead to long term advantage (specifically, a reduced value of the TKE at the end of the optimization period). The idea is akin to allowing sacrifices during a game of chess.

In addition to the selection of  $T$ , the choice of the cost functional to be minimized, which mathematically defines the problem to be solved, is another critical decision which must be made. A discussion of the pros and cons of a variety of different cost functionals is presented in §6.1. Figure 12 shows the performance of the optimized controls for three of the most promising optimal control formulations for  $T^+ = 100$ : specifically, those based on the minimization of  $\mathcal{J}_{\text{DRAG}}$ ,  $\mathcal{J}_{\text{TKE(reg)}}$ , and  $\mathcal{J}_{\text{TKE(ter)}}$ . Over the long term, the  $\mathcal{J}_{\text{TKE(ter)}}$  formulation is clearly superior, and is the only one of the three formulations which relaminarizes this particular flow in our present simulations.

Scaling the DNS-based predictive control approach to higher Reynolds numbers is extremely difficult due to its computational expense. In the present simulations for the larger values of  $T$ , the computational cost is approximately 50 times that of a regular DNS over the same time interval. This expense is due to iterative flow and adjoint computations and the extra flow computations required to optimize the descent parameter  $\alpha$  at each iteration step (see figure 1 and §6.4 for further details). Many techniques have been proposed to streamline the computational algorithm, such as application of the reduced-storage BFGS approach (which would greatly reduce the need for extra flow computations to determine  $\alpha$ ), the solution of several suboptimal problems to precondition the optimal control problem over the full time interval (Heinkenschloss 1999), and the utilization of (cheaper) large-eddy simulations (LES) during the iterative flow prediction and adjoint computation stages of the procedure (Chang & Collis 1999).

However, even with the above-mentioned computational expense of the present approach, figure 13 reveals that the approach can at least be extended to flows at  $Re_\tau = 180$ , leading (in the  $T^+ = 40$  case) to about a 50% drag reduction and a factor of 3 in TKE reduction in 500 viscous time units. This is almost identical to the performance seen in figure 11 for the  $T^+ = 50$  case at  $Re_\tau = 100$  over the same time period (500 viscous time units). Relaminarization of this flow should also therefore be possible with the present approach given a sufficient amount of

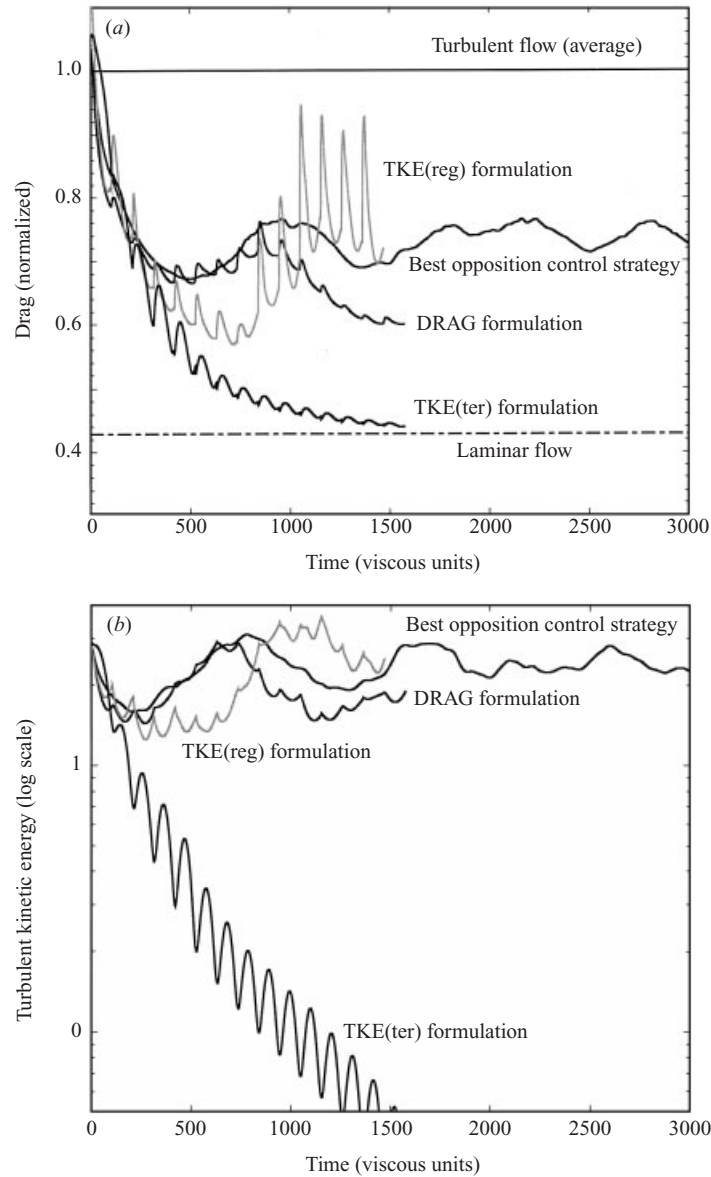


FIGURE 12. Performance of optimized controls for three different optimal control formulations ( $\mathcal{J}_{\text{DRAG}}$ ,  $\mathcal{J}_{\text{TKE}(\text{reg})}$ , and  $\mathcal{J}_{\text{TKE}(\text{ter})}$  as labelled) as computed in direct numerical simulations at  $Re_\tau = 100$ : (a) history of drag, (b) history of turbulent kinetic energy. The optimization horizon was taken as  $T^+ = 100$  for all three optimal control formulations shown here. The best opposition control strategy (from Hammond *et al.* 1998) is shown for comparison.

computer time. As the simulation yielding the lower curves of figures 13(a) and 13(b) took approximately 1500 hours of single-processor Cray C90 time, extending these drag and TKE histories will be deferred until the improved optimization approaches discussed above have been developed. As both  $Re_\tau = 100$  and  $Re_\tau = 180$  should probably be considered as 'low Reynolds number', the question of the ability to scale the present approach to 'high Reynolds number' is left unanswered, though it is clear

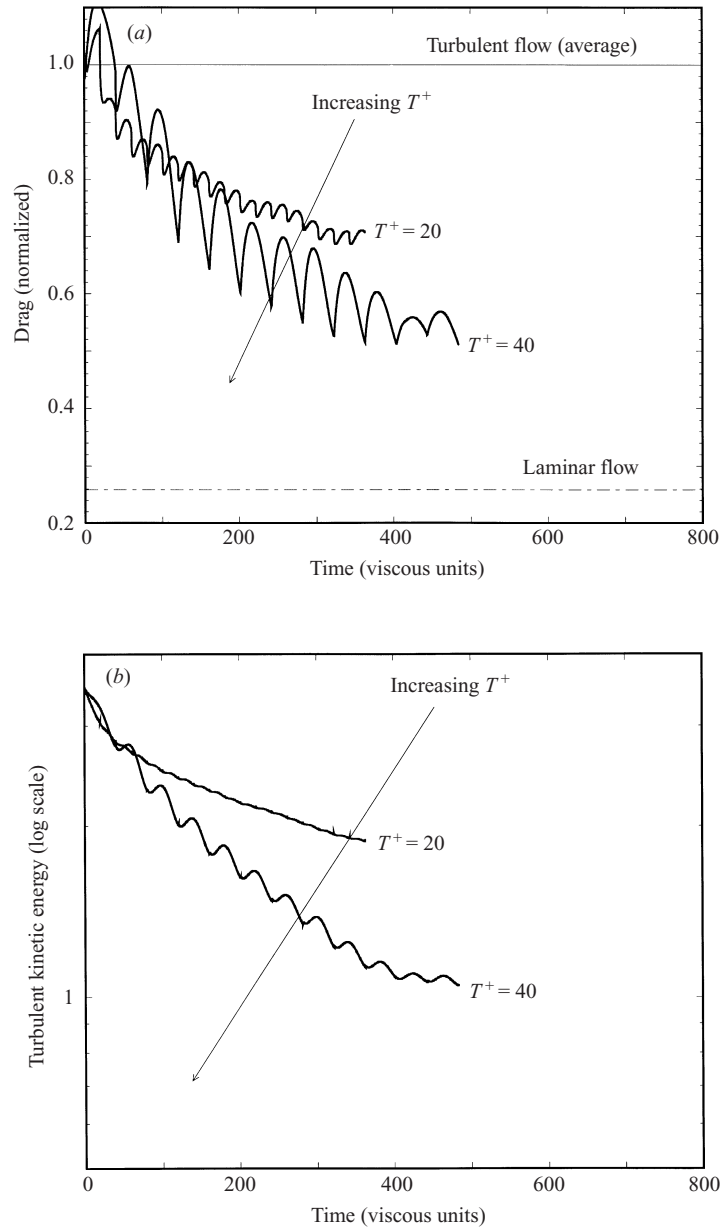


FIGURE 13. Performance of optimized controls for formulations based on  $\mathcal{J}_{\text{TKE}(\text{ter})}$  as a function of the optimization horizon  $T^+$  as computed in direct numerical simulations at  $Re_\tau = 180$ : (a) history of drag, (b) history of turbulent kinetic energy. Again, longer optimization horizons are seen to be superior. Unfortunately, due to the high number of iterations required, the present simulations are approximately 50 times more expensive than regular direct numerical simulations, and thus computations at this Reynolds number are prohibitively expensive with present resources.

that more efficient numerical techniques should be explored before significantly higher Reynolds numbers are considered.

Note that constant-mass-flux channel flows at  $Re_\tau = 100$  and  $Re_\tau = 180$  are both subcritical; once brought to a sufficiently small neighbourhood of the laminar state, these flows will relaminarize with no further control feedback required. Note

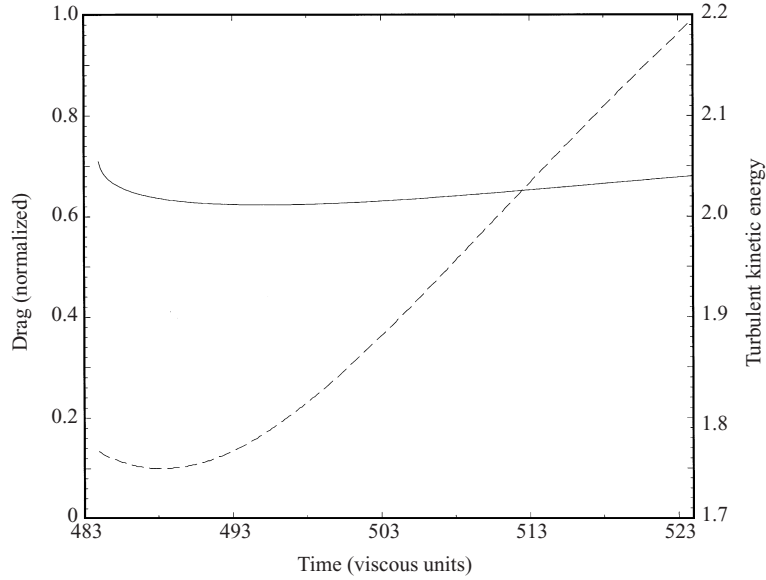


FIGURE 14. Response of system on  $[t, t + T]$  in a controlled simulation ( $\mathcal{J}_{\text{TKE(ter)}}$  formulation,  $T^+ = 40$ , and  $Re_\tau = 180$ ) with control turned off at  $t^+ = 483$ : —, drag (scale at left); ---, TKE (scale at right). The faster rise of the TKE indicates that it is a more sensitive indicator of turbulence regeneration in the flow.

also, however, that laminar channel flows at  $Re_c > 5772$  are readily made linearly stable by linear feedback control strategies (see, for example, the recent work on the development of linear feedback control strategies surveyed by Bewley 2001). Once such linearly stabilizing linear feedback is applied to a higher-Reynolds-number turbulent flow, the system becomes subcritical, just like uncontrolled systems studied in the present manuscript. Further, as discussed in our exposition on possible cost functions in §6.1, and argued by Farrell & Ioannou (1996) and elsewhere, the extraction of energy from the mean flow, and thus the sustenance of the energy feeding the turbulence cascade, is described by mechanisms which might be characterized as ‘primarily linear’. Linear control feedback might thus someday get us much closer to the stabilization of turbulence, if not all the way there. By applying adjoint-based techniques on top of linear control strategies, which take care of the so-called ‘primarily linear’ mechanisms sustaining the turbulent cascade of energy, we might well make the task of controlling turbulence substantially easier. Thus, it makes sense to apply nonlinear adjoint-based control optimization as an add-on on top of linear control feedback which linearly stabilizes the higher-Reynolds-number flow in question. On the other hand, the sheer dynamic complexity of higher-Reynolds-number flows might well prove to be a Gordian knot which is impossible to cut; this exciting question remains, for the moment, unanswered.

To address the question of why the formulation based on minimization of  $\mathcal{J}_{\text{TKE(ter)}}$  worked better than the formulation based on minimization of  $\mathcal{J}_{\text{DRAG}}$ , the control was turned off at  $t^+ = 483$  in one of the controlled simulations. With control off, the turbulence in the flow quickly regenerates and the flow eventually returns to the fully turbulent state<sup>†</sup>. The regeneration of turbulence over the time interval  $[t, t + T]$  is shown in figure 14. As can be seen, the TKE (a measure of the fluctuations in

<sup>†</sup> Note that this is a subcritical flow, but we are still well outside the domain of convergence of the laminar state at this point in the simulation.

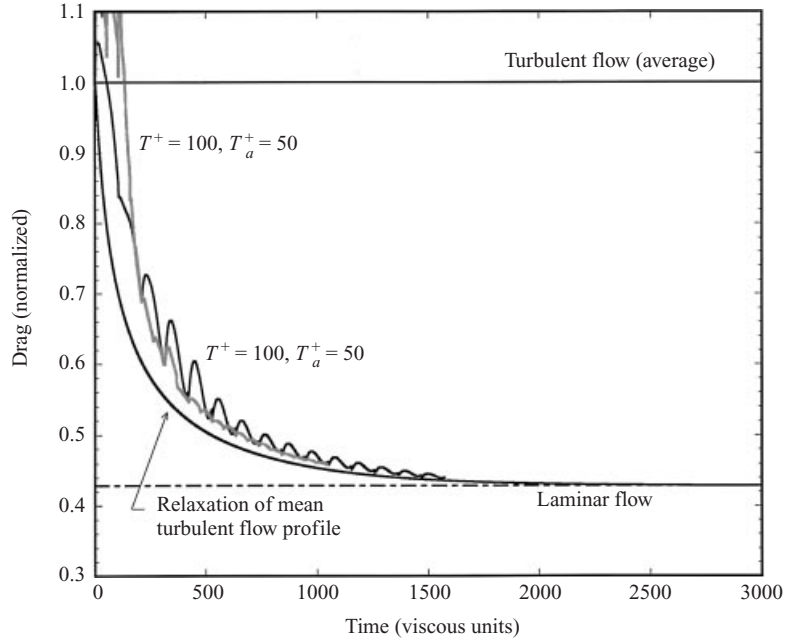


FIGURE 15. Drag of optimized controls for formulations based on  $\mathcal{J}_{\text{TKE}(\text{ter})}$  for  $T^+ = 100$  as  $T_a^+$  is reduced from  $T^+$  to  $T^+/2$ . Also plotted (lower curve) is the relaxation of the mean turbulent flow profile to the laminar state, with all modes other than  $k_x = k_z = 0$  artificially set to zero at  $t = 0$ . The proximity of the three curves implies that the drag reduction performance of the optimized unsteady controls in these cases appears to be nearly ideal.

the flow) responds much more quickly than does the drag (a measure of the mean flow profile) when characterizing the regeneration of turbulence in the flow. This provides numerical evidence for the statement made in §2.1 that turbulence is the ‘cause’ and high drag is the ‘effect’, and it is most effective to target the ‘cause’ in the cost functional.

Figure 15 illustrates that, for the  $\mathcal{J}_{\text{TKE}(\text{ter})}$  case with  $T^+ = 100$ , reducing  $T_a^+$  from  $T^+$  to  $T^+/2$  results in a negligible performance increase. In fact, the drag reduction performance of the controlled system with  $T^+ = 100$  is quite close to what appears to be the fundamental performance limitation set by the time scale of the relaminarizing mean flow profile, shown as the lower curve in figure 15.

In the optimal calculations presented here, we chose  $\ell = 10^{-2}$  (control effort is taken to be ‘cheap’), and the cost functional is dominated in all cases by the contribution of the term which is a function of  $u$ . Note that, for a linear system, small  $\ell$  in the control formulation can result in a very large control magnitude. For the present nonlinear system, it was found that the small  $\ell$  limit actually resulted in a finite control magnitude, with an r.m.s. magnitude of the control approximately equal to that used in the  $y^+ = 15$  opposition control cases discussed in §1.2. Increased values of  $\ell$  resulted in decreased control magnitude and reduced values of drag and TKE reduction.

The spatial correlations of the control distribution are commensurate with the spatial correlations of the flow fluctuations near the wall in both the  $x$ - and  $z$ -directions, exhibiting approximately the classic ‘streak spacing’ when the control is turned on and correlations over longer distances as the flow nears relaminarization.

This result is exactly as expected. In a discrete implementation, actuators some fraction of the streak spacing in the uncontrolled turbulent flow would be necessary to effectively control this system.

The power utilized by the control algorithm is given by the rate of addition of kinetic energy to the flow plus the rate of work done against the (fluctuating) hydrodynamic pressure of the fluid. The straightforward expression for the power applied by the control algorithm on the horizon  $[0, T]$  is

$$\mathcal{P}_\phi = \frac{1}{T} \int_0^T \int_{\Gamma_\pm} \phi \left( \frac{\phi^2}{2} + p \right) \mathbf{d}\mathbf{x} \, dt,$$

whereas the power expense due to the drag of the flow (which is overcome by the mean pressure gradient  $P_x$ ) may be calculated as

$$\mathcal{P}_{DRAG} = \frac{P_x}{T} \int_0^T \int_\Omega u_1 \mathbf{d}\mathbf{x} \, dt.$$

However, the expression for  $\mathcal{P}_\phi$  accounts for both kinetic energy addition to the flow by blowing and also kinetic energy removal from the flow by suction, and the  $p\phi$  work term is not necessarily positive. Note also that, due to the mass flux constraint on the control, (3.2), the mean value of pressure on the wall  $\bar{p}$  does not affect  $\mathcal{P}_\phi$ . In most physical implementations, however, it is unlikely that useful energy can be effectively extracted from the system by the actuators. Our idealization of blowing/suction applied as the actuation is too far removed from the actual application hardware to get a reliable estimate of the power requirements using the above expression for  $\mathcal{P}_\phi$ . Adding absolute value signs in a completely *ad hoc* manner and subtracting out the effect of the mean pressure  $\bar{p}$ , which is unspecified in the current system, a conservative estimate of the power used by an actual control algorithm is

$$\frac{1}{T} \int_0^T \int_{\Gamma_\pm} \left( |\phi| \frac{\phi^2}{2} + |\phi(p - \bar{p})| \right) \mathbf{d}\mathbf{x} \, dt.$$

Even with this conservative formula for estimating the power requirement of the actuators, the power required by the actuators in the present simulations is less than 1% of the power saved due to the drag reduction of the relaminarized flow. Thus we see that the the control authority here is large: it is not by brute force, but rather by finesse, that relaminarization is attained.

## 8. Conclusions

The purpose of this paper is to present the fundamental issues central to the application of optimal control theory in the predictive control framework to the problem of turbulence, and to illustrate the effectiveness of this approach in well-resolved direct numerical simulations of incompressible low-Reynolds-number turbulent channel flows. Primary conclusions include:

1. There is sufficient control authority in small amounts of zero-net-mass-flux blowing and suction distributed intelligently over the walls to completely relaminarize a low-Reynolds-number turbulent channel flow.
2. The DNS-based receding-horizon predictive control framework, in which adjoint fields are used as the central component of a gradient-based optimization strategy, provides a numerically tractable algorithm for computing effective controls. The adjoint field computation is about as expensive as a flow field computation over the same time interval. The Polak–Ribiere variant of the conjugate gradient algorithm,

with occasional resetting to a simple gradient step, is an effective minimization method using this high-dimensional gradient information. The optimizations performed here are, to the best of our knowledge, the highest-dimensional control optimizations ever performed; on each optimization interval in the  $Re_\tau = 180$ ,  $T^+ = 40$  case (for which there were 280 time steps per optimization interval), there were  $170 \times 170 \times 2 \times 280 \approx 10^7$  control variables and  $170 \times 129 \times 170 \times 280 \approx 10^9$  state variables. The expense of the algorithm must be drastically reduced in the future; the purpose of the present simulations was to determine a best-case ‘benchmark’.

3. There is sufficient flexibility in the present method that, with minor modification, it can be used to optimize controls for both regulation and terminal control problems targeting a wide variety of flow quantities of interest, with concentration on large, intermediate, or small length scales. An *a priori* understanding of flow physics may therefore be blended with the mathematical optimization strategy by appropriate selection of the cost functional.

4. Formulations which optimize the controls over longer time horizons  $T$  have a significant advantage over formulations which optimize over shorter time horizons.

5. Formulations based on terminal control strategies, which allow excursions in the short term if they lead to long term advantage, are more effective than formulations based on regulation of the quantity of interest.

6. Formulations based on minimization of drag are less effective than formulations based on the terminal control of turbulent kinetic energy. Drag seems to be a less sensitive indicator of turbulence suppression or regeneration over the time interval than is the terminal value of turbulent kinetic energy.

Though not immediately implementable in hardware, the present work represents a significant step towards the determination of optimally effective yet implementable control strategies for the mitigation or enhancement of the consequential effects of turbulence in flows of real engineering interest. The simulation database resulting in the drag and TKE histories shown in §7 produced hundreds of gigabytes of data which will be combed in future work in an attempt to extract useful correlations which may be exploited by practical control algorithms. Further, based on the groundwork laid in the present paper, the seeds are now sown for the development of practical turbulence control algorithms via adjoint-based optimization of open-loop control parameters and/or the coefficients in implementable feedback control rules.

The authors would like to thank Professors Robert Bitmead, Peter Bradshaw, Haecheon Choi, John Kim, Karl Kunisch, and Mohammed Ziane for important discussions during the course of this work, and Capt. Danforth Bewley for a careful proofread. The first and second authors gratefully acknowledge the funding provided by AFOSR Grant No. F49620-93-1-0078. The third author would like to acknowledge financial support of the National Science Foundation under grant NSF-DMS-9705229 and the support of the Research Fund of Indiana University. The computer time provided by NASA-Ames Research Center and the DoD High Performance Computing Modernization Program at Wright-Patterson Air Force Base in support of this project is also gratefully acknowledged.

## Appendix A. Review: derivation of a simple linear adjoint operator

Consider two scalars  $q(t)$  and  $q^*(t)$  on  $t \in [0, T]$ . Define an inner product such that

$$\langle q, q^* \rangle = \int_0^T q \cdot q^* dt. \quad (\text{A } 1)$$

Let  $\mathcal{N} = \partial/\partial t$ . The adjoint of  $\mathcal{N}$  is found with

$$\langle \mathcal{N}^* q, q^* \rangle = \langle q, \mathcal{N}^* q^* \rangle + b. \quad (\text{A } 2)$$

Using integration by parts,

$$\int_0^T \left( \frac{\partial q}{\partial t} \right) q^* dt = \int_0^T q \left( -\frac{\partial q^*}{\partial t} \right) dt + q q^* |_{t=T} - q q^* |_{t=0}. \quad (\text{A } 3)$$

Thus,  $\mathcal{N}^* = -\partial/\partial t$  and  $b = q q^* |_{t=T} - q q^* |_{t=0}$ .

### Appendix B. Derivation of the adjoint compressible Euler equation

A convenient form of the compressible Euler equation for a perfect gas coupled with a passive scalar equation is

$$\begin{pmatrix} \frac{\partial \rho}{\partial t} + \nabla \cdot \mathbf{m} \\ \frac{\partial \mathbf{m}}{\partial t} + \nabla \cdot \frac{\mathbf{m} \otimes \mathbf{m}}{\rho} + \nabla p \\ \frac{\partial p}{\partial t} + \nabla \cdot \frac{p \mathbf{m}}{\rho} + (\gamma - 1) p \left( \nabla \cdot \frac{\mathbf{m}}{\rho} \right) \\ \frac{\partial \zeta}{\partial t} + \nabla \cdot \frac{\zeta \mathbf{m}}{\rho} \end{pmatrix} = 0. \quad (\text{B } 1)$$

where  $\rho$  is the density,  $\mathbf{m} = \rho \mathbf{u}$  is the momentum vector,  $p$  is the pressure,  $\zeta = \rho \xi$  is the density-weighted passive scalar concentration,  $\gamma$  is a constant, the dot ( $\cdot$ ) denotes the scalar product, and  $\otimes$  denotes the tensor product. The quantities  $\rho$ ,  $p$ , and  $\zeta$  are scalar fields in the domain  $\Omega$  and the quantity  $\mathbf{m}$  is a vector field in the domain  $\Omega$ . In a more compact notation, we will refer to this nonlinear equation simply as

$$\mathcal{N}(\mathbf{q}) = 0 \quad \text{where} \quad \mathbf{q} = \begin{pmatrix} p \\ \mathbf{m} \\ \rho \\ \zeta \end{pmatrix}.$$

Taking the Fréchet derivative of (B 1), it is seen that

$$\begin{pmatrix} \frac{\partial \rho'}{\partial t} + \nabla \cdot \mathbf{m}' \\ \frac{\partial \mathbf{m}'}{\partial t} + \nabla \cdot \left( \frac{\mathbf{m}' \otimes \mathbf{m}}{\rho} + \frac{\mathbf{m} \otimes \mathbf{m}'}{\rho} - \frac{\rho' \mathbf{m} \otimes \mathbf{m}}{\rho^2} \right) + \nabla p' \\ \frac{\partial p'}{\partial t} + \nabla \cdot \left( \frac{p' \mathbf{m}}{\rho} + \frac{p \mathbf{m}'}{\rho} - \frac{\rho' p \mathbf{m}}{\rho^2} \right) \\ + (\gamma - 1) \left( p' \nabla \cdot \frac{\mathbf{m}}{\rho} + p \nabla \cdot \frac{\mathbf{m}'}{\rho} - p \nabla \cdot \frac{\rho' \mathbf{m}}{\rho^2} \right) \\ \frac{\partial \zeta'}{\partial t} + \nabla \cdot \left( \frac{\zeta' \mathbf{m}}{\rho} + \frac{\zeta \mathbf{m}'}{\rho} - \frac{\rho' \zeta \mathbf{m}}{\rho^2} \right) \end{pmatrix} = 0.$$

Note that this equation is linear in the primed variables, and thus we may write it as

$$\mathcal{N}'(\mathbf{q})\mathbf{q}' = 0 \quad \text{where} \quad \mathbf{q}' = \begin{pmatrix} p' \\ \mathbf{m}' \\ \rho' \\ \zeta' \end{pmatrix}.$$

This notation indicates that the equation is linear in  $\mathbf{q}'$ , though the differential operator  $\mathcal{N}'(\mathbf{q})$ , which is found by Fréchet differentiation of the nonlinear operator  $\mathcal{N}(\mathbf{q})$ , is itself a (nonlinear) function of  $\mathbf{q}$ . In tensor form (where the adjoint calculus to be performed is easiest), the differential operation  $\mathcal{N}'(\mathbf{q})\mathbf{q}'$  is written

$$\mathcal{N}'(\mathbf{q})\mathbf{q}' = \begin{pmatrix} \frac{\partial \rho'}{\partial t} + \frac{\partial m'_j}{\partial x_j} \\ \frac{\partial m'_i}{\partial t} + \frac{\partial}{\partial x_j} \left( \frac{m'_j m_i}{\rho} + \frac{m_j m'_i}{\rho} - \frac{\rho' m_j m_i}{\rho^2} \right) + \frac{\partial p'}{\partial x_i} \\ \frac{\partial p'}{\partial t} + \frac{\partial}{\partial x_j} \left( \frac{p' m_j}{\rho} + \frac{p m'_j}{\rho} - \frac{\rho' p m_j}{\rho^2} \right) \\ + (\gamma - 1) \left( p' \frac{\partial}{\partial x_j} \frac{m_j}{\rho} + p \frac{\partial}{\partial x_j} \frac{m'_j}{\rho} - p \frac{\partial}{\partial x_j} \frac{\rho' m_j}{\rho^2} \right) \\ \frac{\partial \zeta'}{\partial t} + \frac{\partial}{\partial x_j} \left( \frac{\zeta' m_j}{\rho} + \frac{\zeta m'_j}{\rho} - \frac{\rho' \zeta m_j}{\rho^2} \right) \end{pmatrix}.$$

We now determine an adjoint operator  $\mathcal{N}'(\mathbf{q})^*$ , which acts on an adjoint state  $\mathbf{q}^*$ , via the identity

$$\langle \mathcal{N}'(\mathbf{q})\mathbf{q}', \mathbf{q}^* \rangle = \langle \mathbf{q}', \mathcal{N}'(\mathbf{q})^* \mathbf{q}^* \rangle + b, \quad \text{where} \quad \mathbf{q}^* = \begin{pmatrix} p^* \\ \mathbf{m}^* \\ \rho^* \\ \zeta^* \end{pmatrix}, \quad (\text{B } 2)$$

and where the inner product is defined such that

$$\langle \mathbf{q}', \mathbf{q}^* \rangle = \int_0^T \int_{\Omega} \mathbf{q}' \cdot \mathbf{q}^* \, dx \, dt.$$

Multiplying out  $\mathcal{N}'(\mathbf{q})\mathbf{q}' \cdot \mathbf{q}^*$ , rearranging, substituting in to the left-hand side of (B 2), and doing the appropriate integrations by parts to move all of the differential operations off of  $\mathbf{q}'$  and onto  $\mathbf{q}^*$ , it is found that

$$\begin{aligned} \mathbf{q}' \cdot \mathcal{N}'(\mathbf{q})^* \mathbf{q}^* &= p' \left( -\frac{\partial \rho^*}{\partial t} - \frac{m_j}{\rho} \frac{\partial \rho^*}{\partial x_j} + (\gamma - 1) \rho^* \frac{\partial}{\partial x_j} \frac{m_j}{\rho} - \frac{\partial m_j^*}{\partial x_j} \right) \\ &+ m'_i \left( -\frac{\partial m_i^*}{\partial t} - \frac{p}{\rho} \frac{\partial \rho^*}{\partial x_i} - \frac{\gamma - 1}{\rho} \frac{\partial}{\partial x_i} \rho^* p - \frac{m_j}{\rho} \frac{\partial m_i^*}{\partial x_j} - \frac{m_j}{\rho} \frac{\partial m_j^*}{\partial x_i} - \frac{\partial p^*}{\partial x_i} - \frac{\zeta}{\rho} \frac{\partial \zeta^*}{\partial x_i} \right) \\ &+ \rho' \left( -\frac{\partial p^*}{\partial t} + \frac{p m_j}{\rho^2} \frac{\partial \rho^*}{\partial x_j} + \frac{(\gamma - 1) m_j}{\rho^2} \frac{\partial}{\partial x_j} \rho^* p + \frac{m_j m_k}{\rho^2} \frac{\partial m_k^*}{\partial x_j} + \frac{\zeta m_j}{\rho^2} \frac{\partial \zeta^*}{\partial x_j} \right) \\ &+ \zeta' \left( -\frac{\partial \zeta^*}{\partial t} - \frac{m_j}{\rho} \frac{\partial \zeta^*}{\partial x_j} \right), \end{aligned}$$

which leads to the following expression for the adjoint operation:

$$\mathcal{N}'(\mathbf{q})^* \mathbf{q}^* = \left( \begin{array}{l} -\frac{\partial \rho^*}{\partial t} - \frac{m_j}{\rho} \frac{\partial \rho^*}{\partial x_j} + (\gamma - 1) \rho^* \frac{\partial}{\partial x_j} \frac{m_j}{\rho} - \frac{\partial m_j^*}{\partial x_j} \\ -\frac{\partial m_i^*}{\partial t} - \frac{p}{\rho} \frac{\partial \rho^*}{\partial x_i} - \frac{\gamma - 1}{\rho} \frac{\partial}{\partial x_i} \rho^* p - \frac{m_j}{\rho} \left( \frac{\partial m_i^*}{\partial x_j} + \frac{\partial m_j^*}{\partial x_i} \right) - \frac{\partial p^*}{\partial x_i} - \frac{\zeta}{\rho} \frac{\partial \zeta^*}{\partial x_i} \\ -\frac{\partial p^*}{\partial t} + \frac{p m_j}{\rho^2} \frac{\partial \rho^*}{\partial x_j} + \frac{(\gamma - 1) m_j}{\rho^2} \frac{\partial}{\partial x_j} \rho^* p + \frac{m_j m_k}{\rho^2} \frac{\partial m_k^*}{\partial x_j} + \frac{\zeta m_j}{\rho^2} \frac{\partial \zeta^*}{\partial x_j} \\ -\frac{\partial \zeta^*}{\partial t} - \frac{m_j}{\rho} \frac{\partial \zeta^*}{\partial x_j} \end{array} \right).$$

Returning to the operator form, the adjoint operation  $\mathcal{N}'(\mathbf{q})^* \mathbf{q}^*$  is written

$$\mathcal{N}'(\mathbf{q})^* \mathbf{q}^* = \left( \begin{array}{l} -\frac{\partial \rho^*}{\partial t} - \frac{\mathbf{m}}{\rho} \cdot \nabla \rho^* + (\gamma - 1) \rho^* \nabla \cdot \frac{\mathbf{m}}{\rho} - \nabla \cdot \mathbf{m}^* \\ -\frac{\partial \mathbf{m}^*}{\partial t} - \frac{p}{\rho} \nabla \rho^* - \frac{\gamma - 1}{\rho} \nabla \rho^* p - \frac{\mathbf{m}}{\rho} (\nabla \otimes \mathbf{m}^* + (\nabla \otimes \mathbf{m}^*)^T) \\ -\nabla p^* - \frac{\zeta}{\rho} \nabla \zeta^* \\ -\frac{\partial p^*}{\partial t} + \frac{p \mathbf{m}}{\rho^2} \cdot \nabla \rho^* + \frac{(\gamma - 1) \mathbf{m}}{\rho^2} \cdot \nabla \rho^* p + \frac{\mathbf{m}}{\rho} \cdot \left( \frac{\mathbf{m}}{\rho} \cdot \nabla \right) \mathbf{m}^* \\ + \frac{\zeta \mathbf{m}}{\rho^2} \cdot \nabla \zeta^* \\ -\frac{\partial \zeta^*}{\partial t} - \frac{\mathbf{m}}{\rho} \cdot \nabla \zeta^* \end{array} \right).$$

The boundary terms which result from the integrations by parts are

$$\begin{aligned} b &= \int_{\Omega} (p^* \rho' + m_j^* m_j' + \rho^* p' + \zeta^* \zeta')|_0^T \, d\mathbf{x} \\ &+ \int_0^T \int_{\partial\Omega} n_j \left[ p^* m_j' + m_i^* \left( \frac{m_j' m_i}{\rho} + \frac{m_j m_i'}{\rho} - \frac{\rho' m_j m_i}{\rho^2} \right) + m_j^* p' \right. \\ &+ \rho^* \left( \frac{p' m_j}{\rho} + \frac{p m_j'}{\rho} - \frac{\rho' p m_j}{\rho^2} + \frac{\gamma - 1}{\rho^2} (\rho p m_j' - \rho' p m_j) \right) \\ &\left. + \zeta^* \left( \frac{\zeta' m_j}{\rho} + \frac{\zeta m_j'}{\rho} - \frac{\rho' \zeta m_j}{\rho^2} \right) \right] \, d\mathbf{x} \, dt, \end{aligned}$$

where  $\mathbf{n}$  denotes a unit outward normal to the surface  $\partial\Omega$  of the domain  $\Omega$ .

#### REFERENCES

- ABERGEL, F. & TEMAM, R. 1990 On some control problems in fluid mechanics. *Theor. Comput. Fluid Dyn.* **1**, 303–325.
- AKSELVOLL, K. & MOIN, P. 1995 Large eddy simulation of turbulent confined coannular jets and turbulent flow over a backward facing step. *Rep. TF-63*. Thermosciences Division, Dept. of Mech. Eng., Stanford University.
- ATKINSON, G. W. 1993 *Chess and Machine Intuition*. Ablex.
- AUBRY, N., HOLMES, P., LUMLEY, J. L. & STONE, E. 1988 The dynamics of coherent structures in the wall region of a turbulent boundary layer. *J. Fluid Mech.* **192**, 115–173.

- BAMIEH, B. 1997 The structure of optimal controllers of spatially-invariant distributed parameter systems. *Proc. 36th IEEE Conf. on Decision and Control, Dec. 8–12, San Diego*.
- BARBU, V. & SRITHARAN, S. S. 1998  $\mathcal{H}_\infty$  control theory of fluid dynamics. *Proc. R. Soc. Lond. A* **454**, 3009–3033.
- BECHERT, D. W., BRUSE, M., HAGE, W. & MEYER, R. 1997 Biological surfaces and their technological application – laboratory and flight experiments on drag reduction and separation control. *AIAA Paper 97-1960*.
- BERKOOZ, G., HOLMES, P. & LUMLEY, J. L. 1993 The proper orthogonal decomposition in the analysis of turbulent flows. *Ann. Rev. Fluid Mech.* **25**, 539–575.
- BEWLEY, T. R. 1999 Linear control and estimation of nonlinear chaotic convection: harnessing the butterfly effect. *Phys. Fluids* **11**, 1169–1186.
- BEWLEY, T. R. 2001 Flow control: new challenges for a new Renaissance. *Prog. Aerospace Sci.* **37**, 21–58.
- BEWLEY, T. R., CHOI, H., TEMAM, R. & MOIN, P. 1993 Optimal feedback control of turbulent channel flow. *1993 Annual Research Briefs*. Center for Turbulence Research, Stanford University/NASA Ames.
- BEWLEY, T. R. & LIU, S. 1998 Optimal and robust control and estimation of linear paths to transition. *J. Fluid Mech.* **365**, 305–349.
- BEWLEY, T. R., MOIN, P. & TEMAM, R. 1996 A method for optimizing feedback control rules for wall-bounded turbulent flows based on control theory. *Proc. ASME Fluids Engng Summer Meeting*. ASME FED, vol. 237, pp. 279–285.
- BEWLEY, T. R., TEMAM, R. & ZIANE, M. 2000 A general framework for robust control in fluid mechanics. *Physica D*, **138**, 360–392.
- BITMEAD, R. R., GEVERS, M. & WERTZ, V. 1990 *Adaptive Optimal Control: The Thinking Man's GPC*. Prentice Hall.
- BLACKBURN, H. M., MANSOUR, N. N. & CANTWELL, B. J. 1996 Topology of fine-scale motions in turbulent channel flow. *J. Fluid Mech.* **310**, 269–292.
- BRYSON, A. E. & HO, Y.-C. 1975 *Applied Optimal Control*. Hemisphere.
- CHANG, Y. & COLLIS, S. S. 1999 Active control of turbulent channel flows based on large-eddy simulation. *Proc. 3rd ASME/JSME Joint Fluids Engng Conf. San Francisco*. FEDSM99-6929.
- CHOI, H., MOIN, P. & KIM, J. 1993 Direct numerical simulation of turbulent flow over riblets. *J. Fluid Mech.* **255**, 503–539.
- CHOI, H., MOIN, P. & KIM, J. 1994 Active turbulence control for drag reduction in wall-bounded flows. *J. Fluid Mech.* **262**, 75–110.
- CHONG, M. S., PERRY, A. E. & CANTWELL, B. J. 1990 A general classification of three-dimensional flow fields. *Phys Fluids A* **2**, 765–777.
- CLARKE, D. 1994 *Advances in Model-Based Predictive Control*. Oxford University Press.
- COLLER, B. D., HOLMES, P. & LUMLEY, J. L. 1994a Control of bursting in boundary layer models. *Appl. Mech. Rev.* **47**, S139–S143.
- COLLER, B. D., HOLMES, P. & LUMLEY, J. L. 1994b Control of noisy heteroclinic cycles. *Physica D* **72**, 135–160.
- CORTELEZZI, L., LEE, K. H., KIM, J. & SPEYER, J. L. 1999 Skin-friction drag reduction via robust reduced-order linear feedback control. *Intl J. Comput. Fluid Dyn.*, submitted.
- DOYLE, J. C., GLOVER, K., KHARGONEKAR, P. P. & FRANCIS, B. A. 1989 State-space solutions to standard  $\mathcal{H}_2$  and  $\mathcal{H}_\infty$  control problems. *IEEE Trans. Auto. Control* **34**, 831–847.
- FARRELL, B. F. & IOANNOU, P. J. 1993 Stochastic forcing of the linearized Navier–Stokes equation. *Phys. Fluids A* **5**, 2600–2609.
- FARRELL, B. F. & IOANNOU, P. J. 1996 Turbulence suppression by active control. *Phys. Fluids A* **8**, 1257–1268.
- FEYNMAN, R. P. 1959 There's plenty of room at the bottom. Presented at the *Annual meeting of the American Physical Society, December 29, 1959*. First published in *Engineering and Science*, Caltech, February 1960.
- FINLAYSON, B. A. 1972 *The Method of Weighted Residuals and Variational Principles*. Academic.
- FURSIKOV, A. V., GUNZBURGER, M. D. & HOU, L. S. 1998 Boundary value problems and optimal boundary control for the Navier–Stokes system: the two-dimensional case. *SIAM J. Control Optim.* **36**, 852–894.
- GAD EL HAK, M. 1996 Modern developments in flow control. *Appl. Mech. Rev.* **49**, 365–379.

- GARCI, C. E., PRETT, D. M. & MORARI, M. 1989 Model predictive control: theory and practice—a survey. *Automatica* **3**, 335.
- GIBSON, C. H. 1996 Turbulence in the ocean, atmosphere, galaxy, and universe. *Appl. Mech. Rev.* **49**, 299–315.
- GREEN, M. & LIMEBEER, D. J. N. 1995 *Linear Robust Control*. Prentice-Hall.
- GUNZBURGER, M. D. (Ed.) 1995 *Flow Control*. Springer.
- GUNZBURGER, M. D., HOU, L. & SVOBODNY, T. P. 1990 A numerical method for drag minimization via the suction and injection of mass through the boundary. In *Stabilization of Flexible Structures* (ed. J. P. Zolesio). Springer.
- HAMMOND, E. P., BEWLEY, T. R. & MOIN, P. 1998 Observed mechanisms for turbulence attenuation and enhancement in opposition-controlled wall-bounded flows. *Phys. Fluids*. **10**, 2421–2423.
- HEINKENSCHLOSS, M. 1997 Optimization methods for optimal control problems. In *Lecture Notes, Summer School on Continuous Optimization, Hamburg-Harburg, Germany, September 22–26*.
- HEINKENSCHLOSS, M. 1999 From suboptimal to optimal control. *Proc. NSF Workshop on Control of Flows, UC San Diego, May 31–June 1*.
- HERTZ, J., KROGH, A. & PALMER, R. G. 1991 *Introduction to the Theory of Neural Computation*. Addison-Wesley.
- HILL, D. C. 1993 Drag reduction at a plane wall. *1993 Annual Research Briefs*. Center for Turbulence Research, Stanford University/NASA Ames.
- HO, C.-M. & TAI, Y.-C. 1996 Review: MEMS and its applications for flow control. *Trans. ASME J. Fluids Engng*, **118**, 437–447.
- HO, C.-M. & TAI, Y.-C. 1998 Micro-electro-mechanical systems (MEMS) and fluid flows. *Ann. Rev. Fluid Mech.* **30**, 579–612.
- HOLMES, P., LUMLEY, J. L. & BERKOOZ, G. 1996 *Turbulence, Coherent Structures, Dynamical Systems and Symmetry*. Cambridge University Press.
- HUNT, J. C. R. & DURBIN, P. A. 1999 Perturbed vortical layers and shear sheltering. *Fluid Dyn. Res.* **24**, 375–404.
- IOANNOU, P. A. & SUN, J. 1996 *Robust Adaptive Control*. Prentice-Hall.
- JACOBS, C. R., SIMO, J. C., BEAUPRÉ, G. S. & CARTER, D. R. 1997 Adaptive bone remodelling incorporating simultaneous density and anisotropy considerations. *J. Biomechanics* **30**, 603–613.
- JACOBS, R. G. & DURBIN, P. A. 1998 Shear sheltering and the continuous spectrum of the Orr-Sommerfeld equation. *Phys. Fluids* **10**, 2006–2011.
- JIMENEZ, J. 1999 The physics of wall turbulence. *Physica A* **263**, 252–262.
- JOSHI, S. S., SPEYER, J. L. & KIM, J. 1997 A systems theory approach to the feedback stabilization of infinitesimal and finite-amplitude disturbances in plane Poiseuille flow. *J. Fluid Mech.* **332**, 157–184.
- KEEFE, L. R. 1993 Drag reduction in channel flow using nonlinear control. *AIAA Paper* 93-3279.
- KEEFE, L. R. 1995 Drag reduction by nonlinear flow control. *NASA CR-195058*.
- KEEFE, L. R. 1997 A normal vorticity actuator for near-wall modification of turbulent shear flows. *AIAA Paper* 97-0547.
- KEEFE, L. R., MOIN, P. & KIM, J. 1992 The dimension of attractors underlying periodic turbulent Poiseuille flow. *J. Fluid Mech.* **242**, 1–29.
- KEPNER, J., PARKER, S. & DECYK, V. 1997 Simulating plasma turbulence in tokamaks. *SIAM News* **30** (4), 1–7.
- KIM, J., MOIN, P. & MOSER, R. 1987 Turbulence statistics in fully developed channel flow at low Reynolds number. *J. Fluid Mech.* **177**, 133–166.
- KOUMOUTSAKOS, P. 1997 Active control of vortex-wall interactions. *Phys. Fluids* **9**, 3808–3816.
- KOUMOUTSAKOS, P. 1999 Vorticity flux control for a turbulent channel flow. *Phys. Fluids* **11**, 248–250.
- KOUMOUTSAKOS, P., FREUND, J. & PAREKH 1998 Evolution strategies for parameter optimization in controlled jet flows. *Proc. 1998 CTR Summer Program*. Center for Turbulence Research, Stanford University/NASA Ames.
- LAGNESE, J. E., RUSSELL, D. L. & WHITE, L. (Eds.) 1995 *Control and Optimal Design of Distributed Parameter Systems*. Springer.
- LEE, C., KIM, J., BABCOCK, D. & GOODMAN, R. 1997 Application of neural network to turbulence control for drag reduction. *Phys. Fluids* **9**, 1740–1747.

- LEE, C., KIM, J. & CHOI, H. 1998 Suboptimal control of turbulent channel flow for drag reduction. *J. Fluid Mech.* **358**, 245–258.
- LIONS, J. L. 1968 *Contrôle Optimal des Systèmes Gouvernés par des Equations aux Dérivées Partielles*. Dunod. (English translation, Springer.)
- LUENBERGER, D. G. 1969 *Optimization by Vector Space Methods*. Wiley.
- LUMLEY, J. L. & BLOSSEY, P. N. 1998 Control of turbulence. *Ann. Rev. Fluid Mech.* **30**, 311–327.
- MAYNE, D. Q. & MICHALSKA, H. 1990 Receding horizon control of nonlinear systems. *IEEE Trans. Auto. Control* **35**, 814–824.
- MCMICHAEL, J. M. 1996 Progress and prospects for active flow control using Microfabricated Electro-Mechanical Systems (MEMS). *AIAA Paper* 96-0306.
- MICHALEWICZ, Z. 1996 *Genetic algorithms + data structures = evolution programs*. Springer.
- MOIN, P. & BEWLEY, T. 1994 Feedback control of turbulence. *Appl. Mech. Rev.* **47** (6), part 2, S3–S13.
- MORSE, P. M. & FESHBACH, H. 1953 *Methods of Theoretical Physics*. McGraw-Hill.
- MUSKE, K. R. & EDGAR, T. F. 1997 Nonlinear state estimation. In *Nonlinear Process Control* (ed. M. A. Henson & D. E. Seborg). Prentice Hall.
- NEWBORN, M. 1997 *Kasparov versus Deep Blue: Computer Chess Comes of Age*. Springer.
- OTT, E. A., GREBOGI, C. & YORKE, J. A. 1990 Controlling chaos. *Phys. Rev. Lett.* **64**, 1196.
- PADMANABHAN, K. T., BOWMAN, C. T. & POWELL, J. D. 1993 Development of an adaptive optimal combustion control strategy. *The Combustion Institute Paper* 93-092.
- PERRY, A. E. & CHONG, M. S. 1987 A description of eddy motions and flow patterns using critical-point concepts. *Ann. Rev. Fluid Mech.* **19**, 125–155.
- PETZOLD, L. R., ROSEN, J. B., GILL, P. E., JAY, L. O. & PARK, K. 1997 Numerical optimal control of parabolic PDEs using DASOPT. In *Large Scale Optimization with Applications. Part II: Optimal Design and Control* (ed. L. Biegler, T. Coleman, A. Conn & F. Santosa). Springer.
- POLAK, E. 1971 *Computational Methods in Optimization*. Academic.
- PRESS, W. H., FLANNERY, B. P., TEUKOLSKY, S. A. & VETTERLING, W. T. 1986 *Numerical Recipes*. Cambridge University Press.
- REUTHER, J., JAMESON, A., FARMER, J., MARTINELLI, L. & SAUNDERS, D. 1996 Aerodynamic shape optimization of complex aircraft configurations via an adjoint formulation. *AIAA Paper* 96-0094.
- SADDOUGH, S. G. & VEERAVALLI, S. V. 1994 Local isotropy in turbulent boundary layers. *J. Fluid Mech.* **268**, 333–372.
- SCALES, L. E. 1985 *Introduction to Non-linear Optimization*. Springer.
- SEBORG, D. E., EDGAR, T. F. & MELLICHAMP, D. A. 1989 *Process Dynamics and Control*. Wiley.
- SOETERBOEK, R. 1992 *Predictive Control: a Unified Approach*. Prentice Hall.
- SRITHARAN, S. S. 1991 Dynamic programming of the Navier–Stokes equations. *Systems and Control Lett.* **16**, 299–307.
- SRITHARAN, S. S. 1998 *Optimal Control of Viscous Flows*. SIAM.
- SUTTON, G. J. & BITMEAD, R. R. 1999 Performance and computational implementation of nonlinear model predictive control. In *Nonlinear model predictive control: assessment and future directions* (ed. F. Allöwer & A. Zheng). Birkhäuser.
- TEMAM, R. 1984 *Navier–Stokes Equations*, Studies in Mathematics and its Applications 2. North-Holland.
- TENNEKES, H. & LUMLEY, J. L. 1972 *A First Course in Turbulence*. MIT Press.
- VAINBERG, M. 1964 *Variational Methods for the Study of Nonlinear Operators*. Holden-Day.
- VANDERPLAATS, G. N. 1984 *Numerical Optimization Techniques for Engineering Design*. McGraw-Hill.
- VILLEMAGNE, C. & SKELTON, R. 1988 Model reductions using a projection formulation. *Int. J. Control* **46**, 2141–2169.
- VOGEL & WADE 1995 Analysis of costate discretizations in parameter estimation for linear evolution equations. *SIAM J. Control Optimiz.* **33**, 227–254.
- YANG, T. H. & POLAK, E. 1997 Moving horizon control of nonlinear systems with input saturation, disturbances, and plant uncertainty. *Int. J. Control* **58**, 875–903.
- ZHOU, K., DOYLE, J. C. & GLOVER, K. 1996 *Robust and Optimal Control*. Prentice-Hall.